



**HAL**  
open science

# Love wave contribution to the ambient vibration H/V amplitude peak observed with array measurements

Brigitte Endrun

► **To cite this version:**

Brigitte Endrun. Love wave contribution to the ambient vibration H/V amplitude peak observed with array measurements. *Journal of Seismology*, 2010, 15 (3), pp.443-472. 10.1007/s10950-010-9191-x . hal-00615403

**HAL Id: hal-00615403**

**<https://hal.science/hal-00615403>**

Submitted on 19 Aug 2011

**HAL** is a multi-disciplinary open access archive for the deposit and dissemination of scientific research documents, whether they are published or not. The documents may come from teaching and research institutions in France or abroad, or from public or private research centers.

L'archive ouverte pluridisciplinaire **HAL**, est destinée au dépôt et à la diffusion de documents scientifiques de niveau recherche, publiés ou non, émanant des établissements d'enseignement et de recherche français ou étrangers, des laboratoires publics ou privés.

Editorial Manager(tm) for Journal of Seismology  
Manuscript Draft

Manuscript Number: JOSE405R1

Title: Love wave contribution to the ambient vibration H/V amplitude peak observed with array measurements

Article Type: SI Array Seismology

Keywords: ambient vibrations, surface waves, array seismology, polarisation analysis, H/V spectral ratio, site characterisation

Corresponding Author: Dr. Brigitte Endrun,

Corresponding Author's Institution: Potsdam University

First Author: Brigitte Endrun

Order of Authors: Brigitte Endrun

**Abstract:** This study applies array methods to measure the relative proportions of Love and Rayleigh waves in the ambient vibration wavefield. Information on these properties is of special relevance for frequencies around the horizontal-to-vertical (H/V) spectral amplitude ratio peak. The analysis of H/V curves, a popular technique in site characterisation, commonly assumes that the curves represent the frequency-dependent Rayleigh wave ellipticity. For the detailed interpretation of amplitudes or the inversion of the curves, it is therefore necessary to estimate and correct for the contribution of other wave types to the ambient vibration wavefield. I use available ambient vibration array measurements to determine the relative amount of Love and Rayleigh waves on the horizontal components by frequency-dependent analysis of the main propagation and polarisation directions, with a special emphasis on the H/V peak frequency as determined from the same recordings. Tests with synthetic data demonstrate the feasibility of this approach, at least in the presence of dominant source regions. Analysis of the data from 12 measurements at nine European sites, which include shallow as well as deep locations that span a wide range of impedance contrasts at the sediment-bedrock interface, indicates that the relative contribution of Rayleigh waves varies widely with frequency, from close to 0% to more than 70%. While most data sets show relative Rayleigh wave contributions between 40% and 50% around the H/V peak, there are also examples where Love waves clearly dominate the wavefield at the H/V peak, even for a site with a low impedance contrast. Longer-term measurements at one site indicate temporal variations in the relative Rayleigh wave content between day- and nighttime. Results calculated with the method introduced herein generally compare well with results of modified spatial autocorrelation analysis. These two methods might be used in a complimentary fashion, as both rely on different properties of the ambient vibration wavefield. This study illustrates that it is possible to measure the relative Rayleigh wave content of the noise wavefield from array data. Furthermore, the examples presented herein indicate it is important to estimate this property, as the assumption that there are an equal proportion of Love and Rayleigh waves is not always correct.

Response to Reviewers: Please refer to the uploaded PDF file ResponsetoReviewersJOSE405.pdf

Journal of Seismology manuscript No.  
(will be inserted by the editor)

# Love wave contribution to the ambient vibration H/V amplitude peak observed with array measurements

Brigitte Endrun

Received: date / Accepted: date

**Abstract** This study applies array methods to measure the relative proportions of Love and Rayleigh waves in the ambient vibration wavefield. Information on these properties is of special relevance for frequencies around the horizontal-to-vertical (H/V) spectral amplitude ratio peak. The analysis of H/V curves, a popular technique in site characterisation, commonly assumes that the curves represent the frequency-dependent Rayleigh wave ellipticity. For the detailed interpretation of amplitudes or the inversion of the curves, it is therefore necessary to estimate and correct for the contribution of other wave types to the ambient vibration wavefield. I use available ambient vibration array measurements to determine the relative amount of Love and Rayleigh waves on the horizontal components by frequency-dependent analysis of the main propagation and polarisation directions, with a special emphasis on the H/V peak frequency as determined from the same recordings. Tests with synthetic data demonstrate the feasibility of this approach, at least in the presence of dominant source regions. Analysis of the data from 12 measurements at nine European sites, which include shallow as well as deep locations that span a wide range of impedance contrasts at the sediment-bedrock interface, indicates that the relative contribution of Rayleigh waves varies widely with frequency, from close to 0% to more than 70%. While most data sets show relative Rayleigh wave contributions between 40% and 50% around the H/V peak, there are also examples where Love waves clearly dominate the wavefield at the H/V peak, even for a site with a low impedance contrast. Longer-term measurements at one site indicate tem-

poral variations in the relative Rayleigh wave content between day- and nighttime. Results calculated with the method introduced herein generally compare well with results of modified spatial autocorrelation analysis. These two methods might be used in a complimentary fashion, as both rely on different properties of the ambient vibration wavefield. This study illustrates that it is possible to measure the relative Rayleigh wave content of the noise wavefield from array data. Furthermore, the examples presented herein indicate it is important to estimate this property, as the assumption that there are an equal proportion of Love and Rayleigh waves is not always correct.

**Keywords** ambient vibrations · surface waves · array seismology · polarisation analysis · H/V spectral ratio · site characterisation

## 1 Introduction

The horizontal-to-vertical (H/V) spectral amplitude ratio technique is a common tool for estimating site effects from ambient vibration recordings. First introduced by Nogoshi and Igarashi (1971) and widely spread by the English publication of Nakamura (1989), this technique involves the calculation of the ratio between the Fourier spectral amplitudes of the horizontal and vertical components of microtremor recordings. The resulting curves often show a clear maximum. The frequency at which this peak occurs is empirically found to correlate with the fundamental resonance frequency at the measurement site (e.g. Lachet and Bard, 1994; Lermo and Chávez-García, 1994; Dravinski et al, 1996). For the case of a single low-velocity layer over a halfspace, Malischewsky and Scherbaum (2004) show theoretically that this correlation is better, the higher the impedance contrast between the layer and the half-space. This method is well suited for rapid site characterisation because it facilitates

B. Endrun  
Institute of Earth and Environmental Sciences, University Potsdam  
Karl-Liebknecht-Str. 24, Building 27  
14476 Potsdam, Germany  
Tel.: +49-331-9775796  
Fax: +49-331-9775700  
E-mail: brigitte.endrun@geo.uni-potsdam.de

the estimation of resonance frequencies, involves only non-invasive measurements with basically a single station, can be conducted quickly (common measurement times at a single location are on the order of ten minutes, e.g. Fäh et al, 2001; Scherbaum et al, 2003; Souriau et al, 2007) and provides reliable results for a wide variety of instrumentation types (Guillier et al, 2008). Thus, H/V measurements are extensively used in microzonation to map the variations in resonance frequencies in densely populated, earthquake-prone areas (e.g. Fäh et al, 1997; Konno and Ohmachi, 1998; Alfaro et al, 2001; Duval et al, 2001; LeBrun et al, 2001; Tuladhar et al, 2004; Panou et al, 2005a; Souriau et al, 2007; Cara et al, 2008; Picozzi et al, 2009; Bonnefoy-Claudet et al, 2009). Bragato et al (2007) propose an algorithm that uses H/V data for the automatic generation of zonation maps for urban areas.

Other applications aim at extracting more information from the H/V spectra using amplitudes and curve shapes. For example, in addition to determining the fundamental resonance frequency, some authors (e.g. Nakamura, 1989; Lermo and Chávez-García, 1994; Konno and Ohmachi, 1998; Panou et al, 2005a) estimate and map amplification levels from H/V data. Scherbaum et al (2003) attempt a formal inversion of H/V curves and find a trade-off between the layer thicknesses and the layer velocities in the resulting models. Hence, they suggest a joint inversion combining the H/V curves with the surface wave dispersion curves derived from array measurements of ambient vibrations at the same location. Several studies have since applied this kind of joint inversion (e.g. Arai and Tokimatsu, 2005; Nagashima and Maeda, 2005; Parolai et al, 2005; Garcia-Jerez et al, 2007; Picozzi and Albarello, 2007; Arai and Tokimatsu, 2008; D'Amico et al, 2008). Others use additional data, for example from borehole or array measurements, to fix either the sediment thickness (e.g. Fäh et al, 2003) or the velocities of the sediment layers (e.g. Yamanaka et al, 1994; Satoh et al, 2001; Arai and Tokimatsu, 2008) and only invert for the respective complementary parameters. Arai and Tokimatsu (2004) conclude, after testing both of these options, that they lead to similar results. Lunedei and Albarello (2009) recently used theoretical modelling to determine that damping also has a non-negligible effect on H/V curves, especially on their amplitudes. They suggest that these curves are potentially useful to determine damping factors, which are otherwise difficult to measure.

Yet, all applications that go beyond mapping peak frequencies make assumptions about which part of the noise wavefield is responsible for the H/V peak. While Nakamura (2000) maintains that the H/V peak is caused by S-wave resonance in the soft surface layer, a growing number of authors agree that the H/V curves correspond to the frequency dependent ellipticity of Rayleigh waves (e.g. Lachet and Bard, 1994; Lermo and Chávez-García, 1994; Ya-

manaka et al, 1994; Konno and Ohmachi, 1998; Fäh et al, 2001; Malischewsky and Scherbaum, 2004; Bonnefoy-Claudet et al, 2006a). These authors argue that surface waves dominate the ambient vibration wavefield, at least above the fundamental resonance frequency of the sedimentary cover (Lunedei and Albarello, 2009). Two recent studies attempt to reconcile these different opinions. They model the H/V curve using the interaction of inhomogeneous surface waves and a surficial low-velocity layer to produce propagating body waves that reverberate within this layer (van der Baan, 2009; Langston et al, 2009). Meanwhile, Bonnefoy-Claudet et al (2006a) report comparable observations of H/V peaks caused by the resonance of S-waves, when they model sources within the bedrock in a similar way. They reason that the ambient vibration wavefield is dominantly man-made for actual measurements, though, and characterised by close and surficial sources. Thus, Bonnefoy-Claudet et al (2006a) conclude that experimental H/V ratios are mainly due to the ellipticity of fundamental mode Rayleigh waves. While the discussion about the theoretical foundations of the H/V peak is ongoing, the most common method is to model H/V spectra (e.g., to invert H/V curves or estimate amplification factors) by using the ellipticity of Rayleigh waves. This method requires a quantitative estimate of the contribution of other wave types to the ambient vibration wavefield, as it is necessary to correct the data for them. Theoretical simulations (Bonnefoy-Claudet et al, 2006a, 2008), as well as comparisons of measured and modelled H/V curves (Arai and Tokimatsu, 2004; Souriau et al, 2007), suggest that the influence of Love waves is significant. For sites with a moderate to strong impedance contrast at the sediment-bedrock interface, modelling shows that the frequency of the Love wave Airy phase is comparable to the H/V peak frequency of the fundamental mode of the Rayleigh wave (Konno and Ohmachi, 1998; Bonnefoy-Claudet et al, 2008). This implies that there may be constructive interference of these two phases in actual measurements. Thus, a large amount of Love waves could greatly increase the measured amplitudes of the H/V peak (Bonnefoy-Claudet et al, 2008). Modelling by van der Baan (2009) shows that, under special circumstances, Love waves may alone be responsible for observed H/V peaks. In addition, variations in the relative content of Love and Rayleigh waves could explain the observed temporal variations in measured H/V amplitudes (e.g. Panou et al, 2005b).

An overview of the literature shows that, when interpreting H/V amplitudes, the relative content of Rayleigh waves is set ad hoc to 50% (Fäh et al, 2001, 2003; Castellaro and Mulargia, 2009), 40% (Konno and Ohmachi, 1998; Arai and Tokimatsu, 2004, 2005, 2008), assumed to be close to 100% (Yamanaka et al, 1994) or not discussed at all (Nagashima and Maeda, 2005; Picozzi and Albarello, 2007; D'Amico et al, 2008). Some authors (e.g. Scherbaum et al, 2003; Paro-

lai et al, 2005) consider scenarios with variable fractions of Love wave energy on the horizontal components but assume that this fraction is stable with frequency. Tokeshi et al (2000) derive the relative Rayleigh wave content of the wavefield at two Japanese sites with available velocity information, by modelling single-station measurements. In order to accomplish this, they try to fit spectral attributes (i.e., amplitude and phase spectra, and the H/V ratio) and the polarisation information from hodograms, by varying the Love to Rayleigh wave ratios of the randomly distributed ambient vibration sources, while also assuming a frequency-independent relationship. In contrast to other reported measurements, they find a relatively large Rayleigh wave content of 64% and 87%.

More recently, a number of authors used array measurements to derive the relative proportion of Rayleigh waves in a wavefield from three-component recordings, either by means of modified spatial autocorrelation (MSPAC) curves (Köhler et al, 2007) or by comparing the energy content on radial and transverse components. They consistently find that Love waves dominate the ambient vibration wavefield. The fraction of Rayleigh waves in various frequency bands lies at 50% or below, sometimes significantly so (see overview in Bonnefoy-Claudet et al, 2006b). At different sites, Rayleigh wave proportions as low as 10% have been observed (Okada, 2003; Köhler et al, 2007). These observations also indicate that the Rayleigh wave content in the ambient vibration wavefield varies with frequency. Similar variations in the theoretical response functions for different modes (Arai and Tokimatsu, 2005) offer an explanation for these findings. The array measurements discussed above have been performed separately from and unrelated to actual H/V measurements. Similarly, if a correction factor is used to model the H/V curves, it is rarely been obtained from actual observations of the wavefield performed concurrently and at the same measurement location as the H/V measurements. This is even the case for studies where array data were actually available (e.g. Satoh et al, 2001; Arai and Tokimatsu, 2008) and not only single station H/V measurements.

Within the EC-projects SESAME (Site EffectS assessment using Ambient Excitations) and NERIES (NEtwork of Research Infrastructure for European Seismology) task JRA4, ambient vibration array measurements were consistently performed at more than 25 locations in Europe. The sites provide a sample of different EC-8 classes, shallow to deep sedimentary layers and urban as well as rural locations. Data from some of these locations show well defined H/V peaks, while other sites display a greater variability in H/V curves, broader peaks or no clear peaks at all. In this contribution, I examine those sites that exhibit clear H/V peaks in more detail. A combination of array analysis, to determine the main direction of wave propagation and polarisation

analysis, is used to derive the relative proportion of Rayleigh waves in the ambient vibration wavefield.

## 2 Methods of Analysis

Previous array studies aimed at measuring the relative Love and Rayleigh wave contents of the ambient vibration wavefield have generally employed either spatial autocorrelation (SPAC) functions or analysis of the energy content of the radial and transverse components (see discussion in Bonnefoy-Claudet et al, 2006b). The SPAC method uses the three components of the azimuthally averaged correlation coefficients to determine surface wave dispersion. In the first step, the frequency-dependent Rayleigh wave phase velocities are estimated from the vertical component of the SPAC curves by grid search (Köhler et al, 2007). With these velocities as additional input, the equations for the horizontal components can be solved, again by grid search. They yield frequency dependent values for the Love wave phase velocity and  $\alpha$ , the relative fraction of Rayleigh waves in the total surface wave content of the horizontal components. Estimates of  $\alpha$  obtained by the three-component MSPAC method (Köhler et al, 2007) are used for comparison in this study.

Some recent advances in the field (e.g., the RayDec method by Hobiger et al (2009) and the FTAN method by Fäh et al (2003)) aim at extracting the pure Rayleigh wave portion of the wavefield from single-station analysis. Only these Rayleigh wave portions are then used for H/V calculations. However, at several sites in Switzerland, Fäh et al (2003) observe a discrepancy between their FTAN results and the traditional H/V curve corrected for 50% Love waves. These discrepancies could either be because there is a larger Love wave content in the wavefield over the whole frequency range considered or because the wavefield lacks suitable wavelets for the FTAN analysis. Based on their method, Fäh et al (2003) cannot distinguish between these two possibilities. Recently, Poggi and Fäh (2009) also suggested the use of high-resolution FK analysis on vertical and radial components of array recordings to extract the relevant part of the wavefield for Rayleigh wave ellipticity calculations, with the added potential of resolving several modes.

Maresca et al (2006) use a different approach and compare the distribution of propagation and polarisation directions in four different frequency bands for two arrays in the Colfiorito Basin, Italy. For one array, they find no clear patterns, while for the other, the approximately normal angle between the propagation and polarisation directions indicates the presence of Love waves in the noise wavefield. This study is based on the same idea. Our observations indicate that the noise wavefield around the H/V peak often exhibits energy concentrations related to distinct sources. These are used to estimate the relative content of Love and Rayleigh waves from the propagation directions obtained by

frequency-wavenumber (FK) analysis and the horizontal polarisation directions. In contrast to the study by Maresca et al (2006), I introduce a quantitative estimate of the relative amount of Love and Rayleigh waves in the wavefield and study the variability of this quantity with frequency, with a special emphasis on the H/V peak frequency. Details of the proposed method are given below.

## 2.1 H/V

H/V curves are calculated in accordance with the recommendations derived during the SESAME project (SESAME, 2005a), using the geopsy software ([www.geopsy.org](http://www.geopsy.org)). Time-windows of 50 s length with 5% overlap are detrended and cosine tapered (taper width of 2.5% or 5% depending on the dataset), then fast Fourier transformed over 100 logarithmically distributed frequency bands between 0.2 and 15 Hz and smoothed using the method proposed by Konno and Ohmachi (1998), with a value of 40 for the smoothing constant  $b$ . Time windows which contain transient signals due to anthropogenic disturbances are deselected. For the remaining time windows, the two horizontal component spectra are combined to yield total horizontal energy before dividing by the vertical component. Then, the geometric mean and standard deviations of the resulting H/V curves are calculated.

## 2.2 Propagation direction

The dominant propagation directions of waves across the array are determined by conventional (beamforming) FK analysis of the ambient vibration wavefield (Lacoss et al, 1969). FK analysis is performed with the geopsy software. The recorded data streams are split into time windows with a frequency dependent length of  $10 \times T$ , with  $T$  being the centre period of the frequency band, and an overlap of 5%. This time-window length is rather short compared to the recommendations by SESAME (2005b), where the use of time windows on the order of  $25 \times T$  to  $50 \times T$  is proposed to reduce the influence of random perturbations to the wavefield. Wathelet et al (2008) confirms for a synthetic dataset that the analysis of longer time windows ( $50 \times T$  vs.  $10 \times T$ ) results in a visibly improved phase velocity estimate. However, the short time-window length is selected here intentionally, considering the requirements for the polarisation analysis. The main polarisation directions are assumed to vary more rapidly and to require a shorter time window for distinct measurements. As polarisation and propagation results are combined in the analysis of the wavefield, it is best to use the exact same time windows for both. Note that in the following analysis of the wavefield composition, no phase velocity information is used. Rather, only the directional information, i.e., the dominant propagation azimuth, from the

FK is extracted for further analysis. As shown below, results for synthetic cases do not show a strong bias in the azimuth data, even for short time windows. The frequency and wave-number range analysed depend on the array response and size. The frequency range is generally split into 100 logarithmically and equally distributed frequency bands for filtering and beam forming. FK analysis is carried out independently for all three components.

## 2.3 Polarisation direction

Polarisation analysis is conducted following Jurkevics (1988). The recorded data are detrended, then band-pass filtered in the same narrow frequency bands as used in the FK analysis and split into the same cosine-tapered time windows of  $10 \times T$  length with 5% overlap. These comparatively short time windows are used because a purely polarised ground motion is assumed within each time window for each frequency band. The polarisation in each time window is found by eigenvalue analysis of the covariance matrix. The covariance matrix can either be considered separately for each of the three-component seismometers or averaged over all sensors within the array (Jurkevics, 1988). The later should lead to a variance reduction in the estimate of the components of the covariance matrix and is thus used herein, but the influence of this parameter on the results is also investigated. No time shifting with respect to propagation velocities across the arrays is performed as, according to Jurkevics (1988), a time-alignment better than  $5 \times T/3$  is required between the different sensors, with  $T$  being the considered period. This criterion gives an upper limit on the resolvable periods, and thus a lower limit on resolvable frequencies, for the case where no time shifting is applied. To agree with this criterion, the minimum distance,  $d$ , between the array stations has to be less than  $5 \times \lambda/3$ , with  $\lambda$  as the corresponding wavelength. However, this is well within the limits of array resolution, as to avoid spatial aliasing,  $d$  has to be less than  $\lambda_{min}/2$ . As a result, the low-frequency limit for determining propagation directions is higher than that for polarisation analysis without any corrections for wave propagation across the array. Evidence for this can also be found in the actual data, where the resolution for determining propagation directions decreases more quickly towards the low frequencies than for determining polarisation directions.

## 2.4 Quantitative estimate of Love wave contribution

For a quantitative estimation of the relative proportions of Love and Rayleigh waves in the wavefield, propagation directions obtained from separate FK analyses of the two horizontal components of motion and horizontal polarisation direction estimates obtained in identical time windows are

used. Propagation directions are determined only from the horizontal components of motion because only the relative proportions of Love and Rayleigh waves in the horizontal components are relevant for correcting the H/V curves. The propagation and polarisation azimuths can then be directly compared to calculate the angular shift between both directions. The average amount of Rayleigh waves in the horizontal components in this frequency band is determined from histograms of the distribution of angular shifts over all time windows for each frequency band. The histograms are calculated for a bin size of  $5^\circ$ . If the histogram shows a distinct maximum around one of the expected angles, the relative amount of Rayleigh waves,  $\alpha$ , is derived from the maximum as explained below. In detail, the requirement for a distinct maximum is specified as a maximum value of the histogram that is more than two times larger than the average value of all bins. A weaker amplitude, or unclear maximum is the result of the sources being randomly distributed, both between and within individual time windows, or of lost resolution of the FK, for example. Fig. 1 a) and d) show examples of frequency windows deselected based on this criterion, where the distribution of samples vs. angular shift looks either random (Fig. 1 a) ) or almost uniform (Fig. 1 d) ). The second criterion specifying the position of the maximum is implemented by requiring the maximum to be located within  $25^\circ$  of the values expected for either a dominant component of Rayleigh waves ( $0^\circ$  or  $180^\circ$ ) or Love waves ( $90^\circ$  or  $270^\circ$ ). Maxima at different angular shifts indicate that neither Love nor Rayleigh waves play a dominant role in the wavefield. These maxima may result from the superposition of wave types, curved wavefronts that are caused by strong sources within or close to the array, or the influence of body waves. Measurements that do not pass these two criteria are discarded.

The absolute values used in the implementation of these criteria are derived from analysis of the synthetic examples, as well as the actual data. Their validity can be checked by considering plots of the histograms of angular shifts between the azimuths of propagation and polarisation directions, as for example shown in Fig. 1. For instance, the range of uncertainty,  $25^\circ$ , is similar to the half-width of the maxima (Fig. 1 b) ). In addition, reasonable estimates of the possible error, introduced by an imperfect horizontal alignment of the sensors and the misalignment of the array, lie well within this range. The threshold values are selected rather conservatively, with the aim of excluding any histogram that shows isolated and random maxima within a single bin. Including these data points would lead to erroneous and insignificant results that are hard to recognise in any later stage of the processing.

For the synthetic, as well as the measured data, variations of the threshold values within reasonable bounds do not result in significant differences in the estimates of  $\alpha$ .

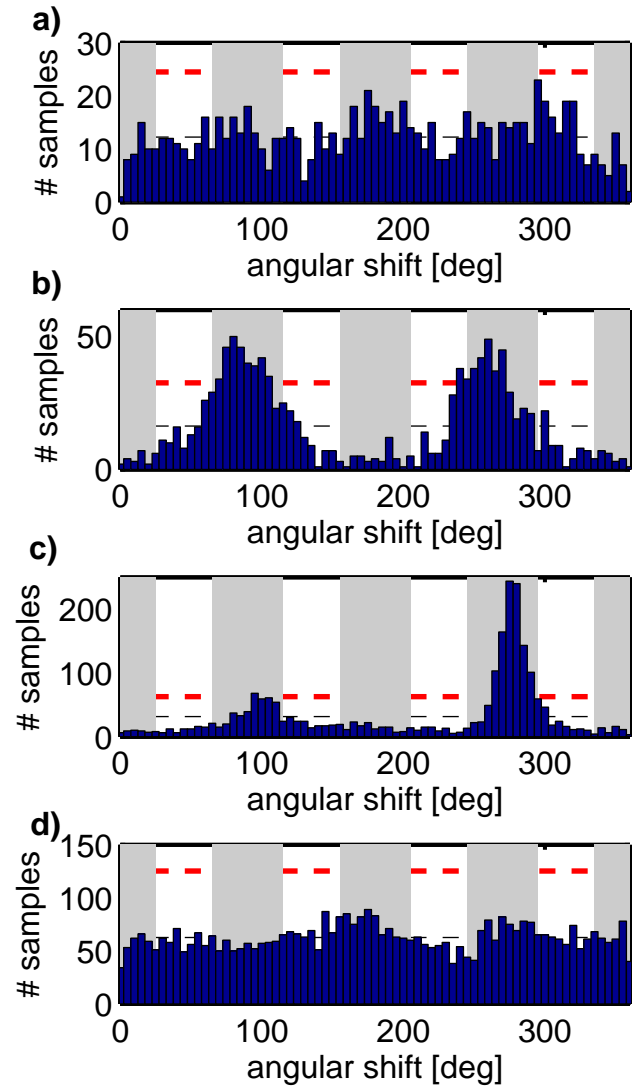


**Fig. 1** Examples of histograms of the angular shifts between the azimuths of the main propagation direction and the horizontal polarisation direction, from which  $\alpha$  is calculated. Examples show results for different frequencies derived from measurements with the largest array deployed at Nestos (compare Fig. 14). In each plot, light grey bars in the background indicate the angular range in which the maximum of the histogram is expected to lie - around  $0^\circ$  or  $180^\circ$  for dominant Rayleigh waves and around  $90^\circ$  or  $270^\circ$  for dominant Love waves. Dashed black lines show the average amplitude levels, while dashed red lines are drawn at twice this value, the threshold for identification of a relevant maximum. a) 1 Hz b) 1.3 Hz (H/V peak frequency) c) 2.5 Hz d) 5 Hz.

However, the estimated standard deviations and the frequencies at which results are considered reliable and accepted are affected. The generally good agreement of the estimated values of  $\alpha$  from different arrays of the actual measurements in the range of their frequency overlap, when available, corroborates the choice of the threshold value (Figs. 14, 18 and 20 a) and d) ). Considering the theoretical limits of resolution of the arrays (Wathelet et al, 2008) might also be helpful in

determining the reliability of the results. Some of the results for the measured data show a conspicuous tendency to converge towards a value of 50% near low frequencies, which might be an indication of resolution lost with this method (Figs. 14 and 20 a), b) and d)).

In applications to real data, the vast majority of the points rejected are the result of filtering using the first criterion, an indistinct maximum in the distribution of the angular shifts. This implies that for actual field cases, at least over the measurement intervals used in this study, there are always frequency bands that do not contain single dominant source regions, but rather random wavefields, which limits the applicability of this method. Rejected points are mainly at the high and low ends of the considered frequency band and thus also exhibit a correlation with the limited resolution of the arrays. Rejections are rarely necessary for the synthetic datasets, if at all.

From the remaining measurements, the relative amount of Rayleigh waves,  $\alpha$  in per cent, is obtained from the amplitudes,  $m$ , of the histograms around angular shifts of  $0^\circ$  and  $180^\circ$  compared to the sum of amplitudes,  $m$ , found around  $0^\circ$ ,  $90^\circ$ ,  $180^\circ$  and  $270^\circ$ , respectively:

$$\alpha = \frac{(m_0 + m_{180}) * 100}{m_0 + m_{90} + m_{180} + m_{270}} \quad (1)$$

An error estimate for  $\alpha$  is computed by independently shifting each frequency bin used in the above calculation by up to five bins (equalling  $25^\circ$ , similar to the range that is allowed to contain the maximum value) in the positive or negative direction and calculating the mean and standard deviation from the  $\alpha$  values that are obtained in each of these 14,641 realisations.

The obtained values of  $\alpha$  can be used to correct the measured H/V curves for the influence of Love waves. Following F ah et al (2003), the amplitude of the horizontal component of the surface wave wavefield is described by vector addition of the Rayleigh wave contribution,  $R$ , on the radial component and the Love wave contribution,  $L$ , on the transverse component. If  $R$  is normalised to 1, the reduction factor,  $c$ , is obtained by

$$c = \sqrt{L^2 + R^2} \quad (2)$$

The dependency on  $\alpha$  can then be expressed by

$$c = \sqrt{\left(\frac{100 - \alpha}{\alpha}\right)^2 + 1^2} \quad (3)$$

For the case of equal Love and Rayleigh contributions to the wavefield, the above equations lead to a value of  $\sqrt{2}$  for  $c$ . Division of the measured H/V curves by  $c$  results in a correction for the Love wave contribution to the horizontal components.

The stability and resolution of the method described above and termed FKPA (FK and Polarisation Analysis), is investigated below, for synthetic, as well as measured data.

### 3 Results

#### 3.1 Synthetic data

The FKPA method was first applied to synthetic data to test it in a controlled environment. The synthetic datasets, approximately 43 minutes long each and sampled at 50 Hz, are calculated for a horizontally layered velocity model (Tab. 1), which is based on borehole data from a shallow urban site in Liege, Belgium (Wathelet, 2005). The array layout considered simulates the following field experiment: three triangles of approximately 10 m, 25 m and 70 m radius rotated by  $40^\circ$  with respect to one another, plus 9 stations on a circle of approximately 50 m radius around a central station, all with the same centre (SESAME, 2002). In the actual field experiment in Liege, different parts of this measurement configuration were consecutively occupied by three different arrays. In the synthetic case, all stations are used together, giving a more idealised response with simultaneous recordings of 19 stations.

Synthetic noise datasets were obtained using the mode summation algorithm of Herrmann (2001) and about 12,500 randomly distributed point sources (single force vectors) of random amplitudes as a background noise environment. The sources are distributed only outside of the array, simulating ideal conditions, in distances between 90 m and 2.2 km from the array centre (black in Fig. 2). To these, approximately 16,100 additional, stronger sources at a distinct location were added. The distinct source region is situated between  $41^\circ$  and  $49^\circ$  at distances between 380 m and 420 m from the array centre (red in Fig. 2). For this source configuration, two data sets were created, one with purely vertical vector sources that contains only Rayleigh waves and one with randomly oriented vector sources that excite Love, as well as Rayleigh, waves. In the first step, only fundamental modes were included in the data set. The effect of higher modes, close sources and more than one dominant source region were also investigated and are discussed below.

**Table 1** Velocity model used in the calculation of the synthetic noise data sets, based on borehole data from the city of Liege.  $h$  refers to layer thickness,  $v_P$  and  $v_S$  to P- and S-wave velocity within the layers. The last layer represents a halfspace at the lower boundary of the model. A constant density of  $2.0 \text{ kg/m}^3$  as well as constant values for  $Q_P$  (250) and  $Q_S$  (100) were used.

$h$ [m]	$v_P$ [m/s]	$v_S$ [m/s]
7.8	310	193
20.0	1112	694
$\infty$	2961	2086

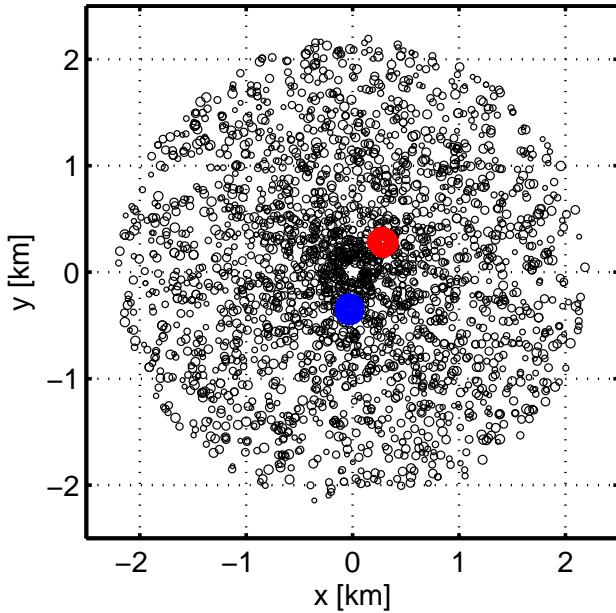


**Fig. 2** Distribution of sources used in creating the synthetic data. For the first part of the calculations, a single dominant source region (red) between  $41^\circ$  and  $49^\circ$  at 380 m to 420 m distance from the array centre was added to a random background distribution (black). To investigate the influence of multiple source regions, a second region (blue) between  $182^\circ$  and  $188^\circ$  at 320 m to 380 m distance was later included. Each circle indicates a point source that was activated randomly up to 10 (background) or 15 (distinct source regions) times. The size of each circle corresponds to the maximum source amplitude, also randomly assigned, that was used at this location. The simulated array of recording stations with a radius of 70 m is centered around (0,0).

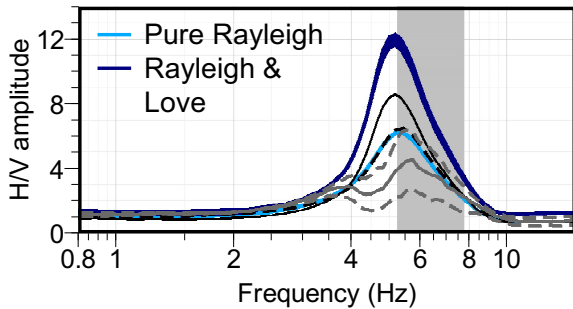


**Fig. 3** H/V curves measured from synthetic data for the Liege model and a noise wavefield that consists purely of Rayleigh or of both Rayleigh and Love waves. The black dashed line is the theoretical Rayleigh wave ellipticity curve calculated for the velocity model in Tab. 1. Solid and dashed grey lines outline the average curve from the Love and Rayleigh wavefield after correcting for the average frequency-dependent Love wave contribution determined by FKPA and its standard deviation (see text for details), while the thin black line is the curve corrected for the standard assumption of equal Love and Rayleigh wave content. The grey bar indicates the position of the Love wave's Airy phase, derived from forward-calculating the group velocity curve for the model.

### 3.1.1 Pure Rayleigh vs. Love-and-Rayleigh data set

Fig. 3 shows the results of the H/V calculations for the two synthetic data sets. As listed in the upper part of Tab. 2 under the label "Synthetics", the maximum amplitude,  $A_0$ , of the H/V peak depends on the contribution of Love waves to the wavefield. It is significantly higher (12.2 vs. 6.2) in the case of randomly oriented source vectors (represented by "L & R FM" in Tab. 2) compared to purely vertical vector sources (described as "R FM" in Tab. 2), which illustrates the Love wave contribution to the H/V peak. The H/V peak frequency also shows some small variation in relation to the existence of Love waves in the wavefield. For the pure Rayleigh wave wavefield, the measured H/V curves agree almost exactly with the fundamental mode Rayleigh wave ellipticity calculated independently from the Liege velocity model (black dashed line). It is interesting to note that the H/V peak frequency around 5.2 Hz is located close to the low-frequency boundary of the Love wave Airy phase (grey shading in Fig. 3) for this velocity model.

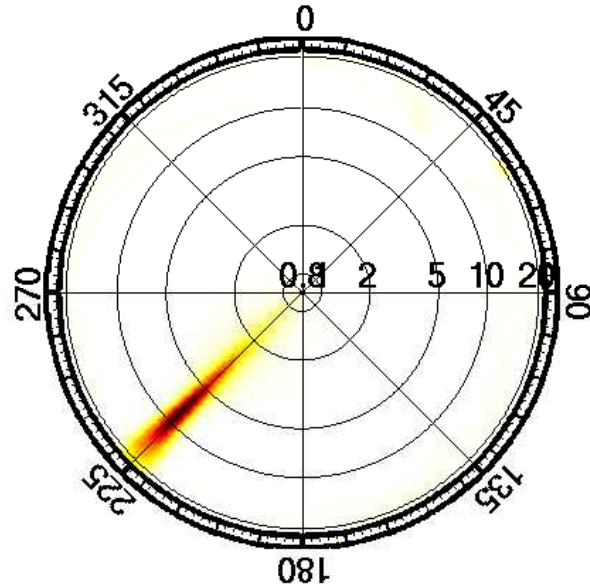


**Fig. 4** Propagation directions found in FK analysis of the synthetic data in the case of purely Rayleigh wave fundamental mode propagation for one dominant source. The radial coordinates give frequency in Hz, from 0.8 to 22. The colourscale represents increased intensity from white over yellow to red. Only the east component is plotted, but north and vertical component both show very similar results.

Fig. 4 shows the result of propagation analysis of the east component of the array recordings for the case of a pure Rayleigh fundamental mode wavefield. FK analyses of the north and vertical components lead to similar results. As expected, the dominant propagation direction is  $225^\circ$  for all frequencies, located at  $180^\circ$  from the known predominant

**Table 2** Results of H/V measurements and available geotechnical information at the nine discussed sites, sorted by increasing H/V peak frequency. Corresponding information for the synthetic dataset is also given (uppermost two rows). Here, R FM refers to the Rayleigh fundamental mode data set, while L & R FM implies the combined Love and Rayleigh fundamental mode data. For the actual measurement sites, code refers to the name code of the respective site in Fig. 9.  $D_{max}$  gives the maximum array dimensions,  $f_0$  and  $A_0$  are the frequency and amplitude of the observed H/V peak, respectively.  $d_{br}$  corresponds to the depth of the bedrock,  $\bar{v}_S$  is the average shear-wave velocity of the sedimentary cover, and  $Z_m$  is the mean impedance contrast as calculated from the borehole velocity profiles. For Korinthos and Norcia, the last three of these entries are not given as the borehole did not reach the bedrock. References for the geotechnical data are also listed.

site	code	experiment	location	$D_{max}$ [m]	$f_0$ [Hz]	$A_0$	$d_{br}$	$\bar{v}_S$ [m/s]	$Z_m$	reference
Synthetics		R FM		$70 \times 70$	5.35	6.2	28	400	6.5	
		L & R FM			5.15	12.2				
Korinthos	K	NERIES	urban	$125 \times 135$	0.48	5.3	N/A	N/A	N/A	Picozzi et al (2007)
Colfiorito E	C	SESAME	rural	$220 \times 220$	0.65	16.9	61	160	7.6	Di Giulio et al (2006)
Colfiorito	C	NERIES	rural	$165 \times 180$	0.65	16.8	61	160	7.6	Di Giulio et al (2006)
Volvi	V	NERIES	rural	$710 \times 780$	0.7	8.9	196	430	7.6	Raptakis et al (2000)
Volvi	V	SESAME	rural	$380 \times 420$	0.7	8.7	196	430	7.6	Raptakis et al (2000)
Colfiorito B & D	C	SESAME	rural	$220 \times 220$	0.9	9.8	52	160	10.8	Di Giulio et al (2006)
Thessaloniki	T	SESAME	urban	$235 \times 395$	1.0	10.2	150	530	5.4	Anastasiadis et al (2001)
Nestos	N	NERIES	rural	$165 \times 175$	1.3	16.8	52	330	4.0	Picozzi et al (2007)
Cereto di Spoleto	CS	NERIES	outskirts	$145 \times 160$	2.2	8.1	24	425	3.4	Picozzi et al (2007)
Athens	A	NERIES	urban	$90 \times 115$	3.9	3.0	30	520	1.9	Picozzi et al (2007)
Aigio (A & B)	AI	NERIES	urban	$65 \times 80$	5.7	3.8	20	430	3.5	Athanasopoulos et al (1999)
Norcia	NC	NERIES	outskirts	$230 \times 255$	8.0	5.8	N/A	N/A	N/A	Picozzi et al (2007)

source direction ( $45^\circ$ ). The amplitudes indicate that most of the source energy is radiated at high frequencies, i.e., above 3 Hz. This is consistent with the amplitude spectra of the synthetic seismograms, which manifest the largest amplitudes between 5 Hz and 10 Hz. Although amplitudes remain above 25% of the maximum up to the aliasing limit of the dataset (25 Hz), the spectra show a sharp drop in radiated energy towards lower frequencies, with amplitudes below 10% of the maximum at 4 Hz and below. The results of the propagation analysis are similar when the wavefield contains both Love and Rayleigh waves.

The results of polarisation analysis using all array stations, for both the case of pure Rayleigh wave sources and a wavefield that contains both Rayleigh and Love waves, are displayed in Fig. 5. For the pure Rayleigh wave case, the estimated horizontal polarisation directions for all frequencies are concentrated between  $220^\circ$  and  $225^\circ$ , showing a good agreement with the main propagation direction (Fig. 4), as expected. Because the directions are not focused exactly on an angle of  $225^\circ$ , it suggests there is a small ( $5^\circ$ ) systematic bias in the estimated polarisation directions. This bias may be related to the spatial extension of the distinct source region and the actual distribution of the background sources, which is random, not uniform. As the later analysis allows for an uncertainty of up to  $25^\circ$ , this bias should not influence the results. For the dataset that contains both Rayleigh and Love waves, two main polarisation directions are found. One direction is close to  $45^\circ$ , the other close to  $135^\circ$ . Due to the  $180^\circ$  periodicity in polarisation, the energy around  $45^\circ$  shows the same orientation as the dominant wave propagation direction, and the energy clustered around  $135^\circ$  has a  $90^\circ$  phase shift to the propagation direction, which is char-

acteristic of Love waves. Consequently, both wave types can be resolved in this case.

Fig. 6 shows the distribution of propagation and polarisation directions for the case of Love and Rayleigh waves around the H/V peak frequency at 5.15 Hz, using the five frequency bins centred on this frequency (4.8 Hz to 5.6 Hz). Propagation directions from FK analysis of both horizontal components are depicted together. As already visible in Fig. 5, the main polarisation direction (orange) is at  $90^\circ$  from the main propagation direction (blue) in this frequency range, indicating a dominance of Love waves.

The estimates of the Rayleigh wave content,  $\alpha$ , resulting from FKPA are shown in Fig. 7, which also includes the MSPAC results for comparison. The standard deviation boundaries for  $\alpha$  determined by MSPAC are quite large, which is due to the way  $\alpha$  is determined. The best solution to the equations linking the measured average spatial autocorrelation functions with Rayleigh and Love phase velocities and  $\alpha$  are found by grid-search and the standard deviations are derived from the width of the corresponding minima (Köhler et al, 2007). Moreover, values of  $\alpha$  are determined only with an accuracy of 5% due to the discrete sampling of the grid-search. Significant scattering in the values of  $\alpha$  indicates the frequencies where resolution is lost in MSPAC, i.e., above approximately 11 Hz and below approximately 4.5 Hz, for both pure Rayleigh as well as Love and Rayleigh wavefields.

The distributions of  $\alpha$  with frequency, as determined by FKPA, show a generally good agreement with the MSPAC results. For the pure Rayleigh wavefield, values above 90% Rayleigh wave content are recovered between 1.2 and 10 Hz. At higher frequencies, standard deviations sharply in-

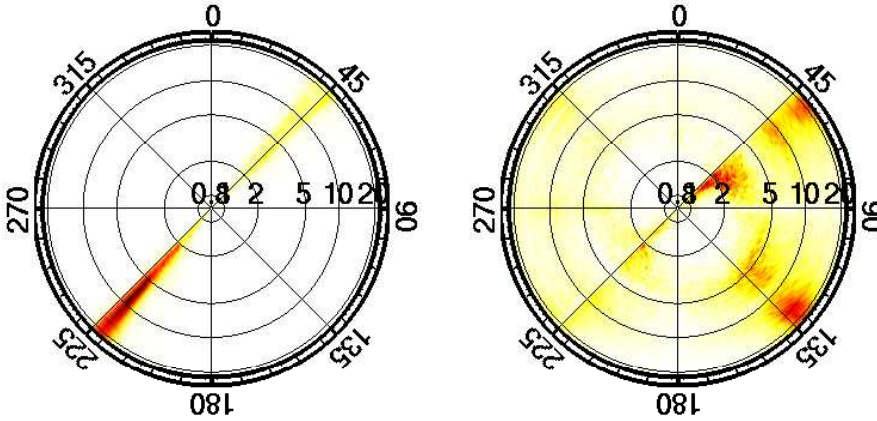


**Fig. 5** Horizontal polarisation directions derived from the synthetic datasets consisting of only Rayleigh waves (left) and both Love and Rayleigh waves (right), displayed as in Fig. 4. Amplitudes below 2 Hz, which would otherwise dominate the figure, are downscaled by half.

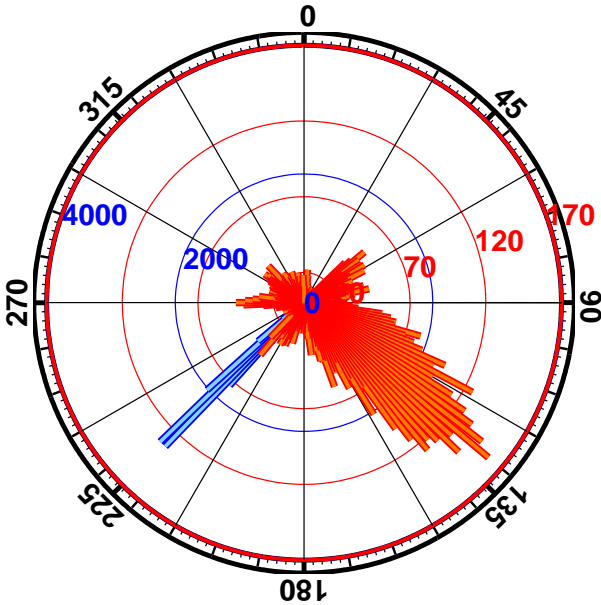


**Fig. 6** Polarisation (orange) vs. propagation (blue) directions measured for the synthetic data for a fundamental mode Love and Rayleigh wavefield in the frequency band between 4.8 and 5.6 Hz, which encompasses the H/V peak.

crease (from an average of 6% to an average of 20%), indicating a decrease in resolution. However, it seems possible to make measurements at lower frequencies than with the MSPAC method. The estimated Rayleigh wave content around the H/V peak frequency is  $97\% \pm 6\%$  from FKPA and  $95\% \pm 10\%$  from MSPAC.

For the combined Rayleigh and Love wavefield, both methods to determine  $\alpha$  also agree widely and indicate variations in  $\alpha$  with frequency. The  $\alpha$  value at the H/V peak frequency, derived from FKPA, is  $26\% \pm 10\%$ , while MSPAC yields a result of  $35\% \pm 15\%$ . Both methods show a clear minimum in  $\alpha$  around 4.5 Hz, with a Rayleigh wave content of less than 25% and a local maximum around 9 Hz, with more than 50% of Rayleigh waves in the wavefield. This maximum is related to the Rayleigh wave Airy phase. Similar to the occurrence of the minimum at frequencies slightly lower than the H/V peak frequency, the maximum occurs at frequencies somewhat below the trough in the H/V curve, which is measured around 10.8 Hz. Approaching the low frequencies, the results from FKPA are more stable than the MSPAC results and indicate a large amount (close to 90%) of Rayleigh waves in the horizontal wavefield, whereas approaching the high frequencies, the estimates for  $\alpha$  seem to level off around 50%. Using only a single station for the polarisation analysis, instead of averaging over the whole array, usually results in a change of less than 5% for  $\alpha$ . This is the case for both, the pure Rayleigh and the combined Rayleigh and Love wavefield. However, for single stations and individual frequencies, larger outlier values, of up to 17%, are observed.

As an independent test of these results, the range of values for  $\alpha$  that were determined at each frequency by FKPA are used to correct the H/V curve, measured for the synthetic Love and Rayleigh dataset, for the contribution of Love waves to the horizontal spectra, as described in 2.4. The resulting curves (grey lines in Fig. 3) should compare to the H/V curve for the pure Rayleigh case. At frequencies

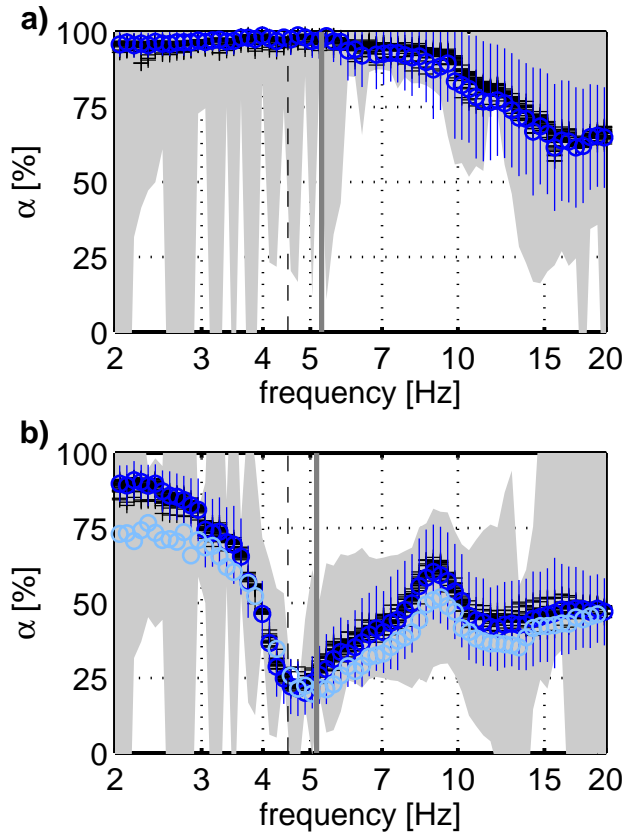


**Fig. 7** Measured values of the Rayleigh wave content  $\alpha$  for the synthetic datasets in the case of a) pure Rayleigh sources and b) combined Rayleigh and Love sources. Light grey shading indicates the standard deviation boundaries for the  $\alpha$  values determined by MSPAC. Black crosses give average values of alpha using polarisation analysis for each individual station, while blue circles with standard deviations are the values derived with polarisation measurements averaged over the whole array. Dark grey lines mark the frequency of the H/V peak. Thin dashed black lines mark the theoretical lower resolution limit of the array. Light blue circles in b) give the result for the case of two dominant source regions for comparison.

above 6.5 Hz and below 4 Hz, the curve corrected with the average value of  $\alpha$  at each frequency consistently follows the H/V curve measured for the synthetic pure Rayleigh case. Between 6.5 Hz and 4 Hz, which is precisely the region of the H/V peak frequency, the H/V curve for Rayleigh waves more closely follows the maximum curve, which was determined by adding one standard deviation to the calculated values of  $\alpha$ . Also, a deviation in the shape of the corrected H/V curve from the measured Rayleigh wave curve is found between 4.2 Hz and 5.3 Hz. Here, the shape of the corrected curves is distorted due to the minimum in  $\alpha$  measured around 4.5 Hz. This also affects the peak frequency of the corrected maximum curve. At 5.6 Hz, it is slightly larger than 5.35 Hz, which is the H/V peak frequency obtained from analysis of the synthetic Rayleigh wave data set. The

match in amplitude between the maximum corrected curve and the measured curve is very close (6.3 vs. 6.2), however.

The fact that the maximum corrected curve, rather than the average  $\alpha$ -corrected curve, is closer to the measured curve might reveal a bias in the method. In the case discussed here, the average value of  $\alpha$  at the peak frequency determined by MSPAC (which at 35% is close to the average value of FKPA plus one standard deviation, 25% + 10%) is closer to the true value. However, with FKPA, a meaningful determination of  $\alpha$  appears to be possible to lower (at least down to 1 Hz) and higher (at least up to 15 Hz) frequencies than with the MSPAC method. The FKPA results around the H/V peak are resistant to changes in the threshold values that are used to calculate  $\alpha$ , as well as variations in the synthetic Love and Rayleigh wavefield, some of which are described in more detail below. The calculation of the corrected curves also suggests that a small uncertainty in  $\alpha$  can result in a large range of possible H/V values. The results derived from the measured data argue against a systematic bias between  $\alpha$  values determined by FKPA and MSPAC. In some cases, the value of  $\alpha$  determined by FKPA for the H/V peak frequency is smaller than the value determined by MSPAC (i.e., Nestos). Yet at other sites (i.e., Colfioritoi, Athens C), the opposite is the case, and some cases (i.e., Athens D) show identical results from both methods. Across the whole frequency bands considered, the results from FKPA are located near either the lower or upper limits of the values allowed by MSPAC (e.g. Fig. 14). The discrepancy observed in the synthetic test may be related to the specifics of the synthetic wavefield and warrants further investigation. From these results, it appears necessary to consider the entire range of values within two standard deviations when applying the method in its current form. A comparison of our results to those from correcting the measured H/V curve with the standard assumption of a Rayleigh wave content of 50% (Fig. 3 thin solid black line) indicates that the standard assumption is inaccurate around the H/V peak. In fact, because the values required for correction vary between 90% and 30%, a good match cannot be expected when using any single value of  $\alpha$  for all frequencies.

### 3.1.2 Close sources

To investigate the influence of the source-free region in close vicinity to the recording stations, a dataset with background sources randomly distributed between 0 m and 2.2 km from the array centre was created. In contrast to the case presented before (3.1.1), where no sources are located closer than 90 m to the array centre, this synthetic example includes background sources located within the array. Adding close sources significantly increases the curvedness of the recorded wavefronts. This violates the assumption made in FK processing, of a plane wave front moving across the ar-

ray. Distributions of the main propagation and polarisation directions for the simulation including close sources are very similar to the results shown in Fig. 4 and 5. The estimates of  $\alpha$  are close to those obtained without close sources (Fig. 7), e.g.,  $\alpha$  equals  $28\% \pm 9\%$  at the H/V peak frequency. Significant deviations towards lower values of  $\alpha$  (around 70%) are observed only for frequencies below 3 Hz. Any measurement in this range might be problematic because the energy in the synthetic wavefield is greatly reduced at low frequencies. However, the H/V curves calculated from the data including close sources, also show a deviation from the dataset without close sources in this frequency range. Below 3 Hz, the H/V curves are approximately flat and the amplitudes are larger for the dataset including close sources (approximately 1.8 vs. 1.3). This indicates that the smaller value of  $\alpha$  for this case could be the result of a variation in the data with close sources, i.e., there is a higher Love wave content at low frequencies. Close sources might change the Love wave content in the dataset because Love waves are more strongly reduced in amplitude during propagation due to the higher damping values for S-waves. Therefore, decreasing the distance to the source could effectively increase the proportion of Love waves that is observed. This effect should be strongest for the largest wavelengths.

### 3.1.3 Higher modes

The actual distribution of various modes in the ambient vibration wavefield is rarely studied and depends on local site and source properties (Bonney-Claudet et al, 2006b). Several studies do, however, indicate that higher modes may be of importance, for example in obscuring the trough in the H/V curve associated with the Rayleigh fundamental mode Airy phase, or for the inversion of dispersion curve data (Bonney-Claudet et al, 2006b). The conventional implementation of SPAC (Aki, 1957) and MSPAC techniques are confined to the resolution of single mode Rayleigh and Love waves (Bonney-Claudet et al, 2008). Accordingly, a theoretical investigation using the MSPAC method (Köhler et al, 2007) indicates that estimates of  $\alpha$  deteriorate at frequencies where higher modes dominate the wavefield. On the other hand, because FK methods have the potential to resolve several surface wave modes simultaneously (Poggi and Fäh, 2009), the FKPA method might have advantages over the MSPAC method at these conditions. A dataset that contains both fundamental and higher modes was created to investigate this point.

Distributions of the main propagation and polarisation directions, including higher modes, are very similar to the results shown in Fig. 4 and 5. The estimates of  $\alpha$  also closely follow the values determined for the fundamental mode case (Fig. 7), e.g.,  $\alpha$  equals  $23\% \pm 10\%$  at the H/V peak frequency. In contrast to the case of close sources, a deviation

is only apparent at high frequencies between 12 Hz and 15 Hz, where values of  $\alpha$  locally show an increase of approximately 10% compared to the fundamental mode case. However, these variations are well within the standard deviation of the fundamental mode dataset, which is approximately 15% at the frequencies considered. A comparison of H/V curves with the dataset containing only fundamental modes exhibits no distinct differences. Accordingly, the observed discrepancy in  $\alpha$  at high frequencies probably does not reflect a property of the data but indicates a bias in the FKPA measurement, likely introduced by the dominance of higher modes at high frequencies. Still, this discrepancy is significantly smaller than the variation in  $\alpha$  of over 30% observed in the MSPAC study by Köhler et al (2007) in the case of a multi-modal wavefield.

### 3.1.4 A second source region

The effect of source distribution was investigated by adding a second concentrated region of randomly activated strong sources. It is located between  $182^\circ$  and  $188^\circ$  at distances 320 m to 380 m from the array centre (Fig. 2, blue). The maximum source amplitude in this second, closer region is three quarters that of the original source region. The distribution of main propagation directions in this case, shows two maxima around the azimuths of the two source regions. For a pure Rayleigh wave wavefield, the distribution of the polarisation directions also shows two maxima at the corresponding azimuths but also exhibits some smearing between them. Estimation of  $\alpha$  at the H/V peak frequency is comparable to the result for a single dominant source region at  $97\% \pm 2\%$ . However, a correct estimation ( $\alpha$  larger than 90%) is only possible in the limited frequency range between 5 Hz and 10 Hz. At higher and lower frequencies, the results quickly degrade to lower values of  $\alpha$ .

For a combined Love and Rayleigh wavefield, it is no longer possible to resolve the complete set of four different polarisation directions contained in the data (Fig. 8). For frequencies below 4 Hz, only one direction is resolved at all by energetic maxima around  $45^\circ$  and  $225^\circ$ , indicating the Rayleigh wave component of the first source region. For higher frequencies, a broad region of smeared energy is located between  $90^\circ$  and  $135^\circ$ , and, slightly more localised in frequency, also between  $45^\circ$  and  $90^\circ$ . This indicates an overlap between the Love wave phases of both source regions, as well as an overlap between the Rayleigh wave phase of the first and the Love wave phase of the second source region. An additional concentration of energy is observed around  $270^\circ$ , related to the Love wave phase of the new, second source region around  $185^\circ$ . Dominance of Rayleigh waves at low frequencies is also visible for the simulation with a single source (Figs. 5 and 7) and is thus probably inherent to the way the synthetic noise data are calculated. Even though

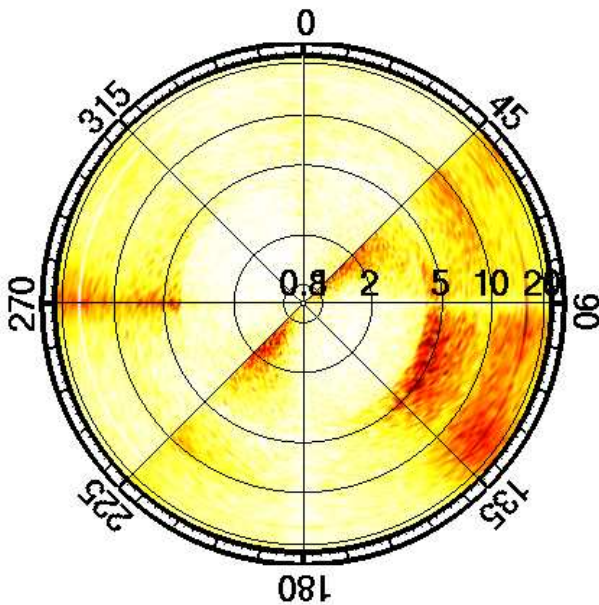


**Fig. 8** Polarisation directions found in FK analysis of the synthetic data in the case of a wavefield composed of Rayleigh and Love waves propagating from two dominant source regions, displayed as in Fig. 4. Results for frequencies below 4 Hz, which would otherwise dominate the picture, are downscaled by half.

it is not possible to distinguish the individual polarisation directions for frequencies above 4 Hz, the estimate of  $\alpha$  at the H/V peak frequency of 5.15 Hz at  $22\% \pm 7\%$  is still very close to the result from the dataset with one dominant source region. Estimates of  $\alpha$  show a general bias toward lower values above 5 Hz, but the difference with the original estimates is, on average, only 6% and well within the standard deviation of the original values (Fig. 7). For frequencies below 3 Hz, the estimated Rayleigh wave content shows a significant shift toward lower values. This can be explained by the period-dependent time window used in the FK and polarisation analyses. As the time window length increases for lower frequencies, the probability that strong sources are active at both of the two locations within the same time window also increases. This adversely affects the estimates of  $\alpha$ , because different, but simultaneously acting, sources are difficult to resolve by the FKPA method.

The described observations indicate that the simultaneous activity of two strong sources, while preventing a clear identification of all polarisation directions contained in the wavefield when averaging over the whole time period (Fig. 8), still allows for an acceptable estimate of the Rayleigh wave contribution to the wavefield, especially around the H/V peak frequency and at higher frequencies, in this special case (Fig. 7). However, using a completely random wavefield (i.e., only a large number of background sources), reduces the effectiveness of the method. For both a pure Rayleigh, as well as a combined Love and Rayleigh wavefield, no

distinct maxima in the distribution of the propagation vs. polarisation directions are observed for most of the covered frequency band, including the H/V peak, and therefore, no measurements are possible. Between 8 Hz and 15 Hz, some results are generated which are within the standard deviation of the original results, but systematically offset to higher (Love and Rayleigh wavefield) or lower (pure Rayleigh wavefield) values. The strong energy radiation associated with the Rayleigh wave Airy phase might be the reason that measurements are possible in exactly this frequency range. These observations show that in the case of a completely random wavefield, the FKPA method is of only limited use. Under these circumstances, using MSPAC might be advantageous, as this method assumes a random wavefield. In fact, all of the simulations conducted by Köhler et al (2007) to measure  $\alpha$  with MSPAC use only completely random wavefields.

### 3.2 Field measurements

Ambient vibration array measurements at more than 25 different locations in Greece, Italy and Turkey were carried out within the two projects SESAME and NERIES. Similar equipment was used for all measurements, consisting of Lennartz Le3D 5s sensors and MarsLite (SESAME) or EarthData (NERIES) digitisers. For the SESAME measurements, 13 seismometers were available that were used to build a single large array (aperture between approximately 200 and 400 m, depending on location) at each site (SESAME, 2002). The NERIES measurements were carried out with eight sensors, seven of which were deployed in an approximately circular shape around a central station. At each site, between two and four arrays of increasing size were deployed (see Endrun and Renalier, 2008, for details). Wireless communication between the stations in the field allowed not only for on-site data quality control but also for preliminary data analysis (Ohrnberger et al, 2006). Accordingly, the optimum size of the consecutive arrays could be efficiently determined from the partial dispersion curve branches available in situ. The measurement duration for each array was at least 45 min and increased with increasing array size. At two locations, measurements were conducted during both experiments, i.e., Volvi and Colfiorito (Tab. 2, Fig. 9). In Colfiorito, arrays were deployed at different locations during SESAME. The location of array E matches the location of the NERIES deployment (Endrun et al, 2009), and arrays B and D occupy the same location but during different times of two consecutive days. In addition, the recordings of array D and E each lasted for more than 12 hours, permitting an investigation of the temporal variability of  $\alpha$  (see section 3.2.3).

Fig. 10 shows the H/V curves for the 13 measurements that exhibit a clear and consistent H/V peak, and Tab. 2

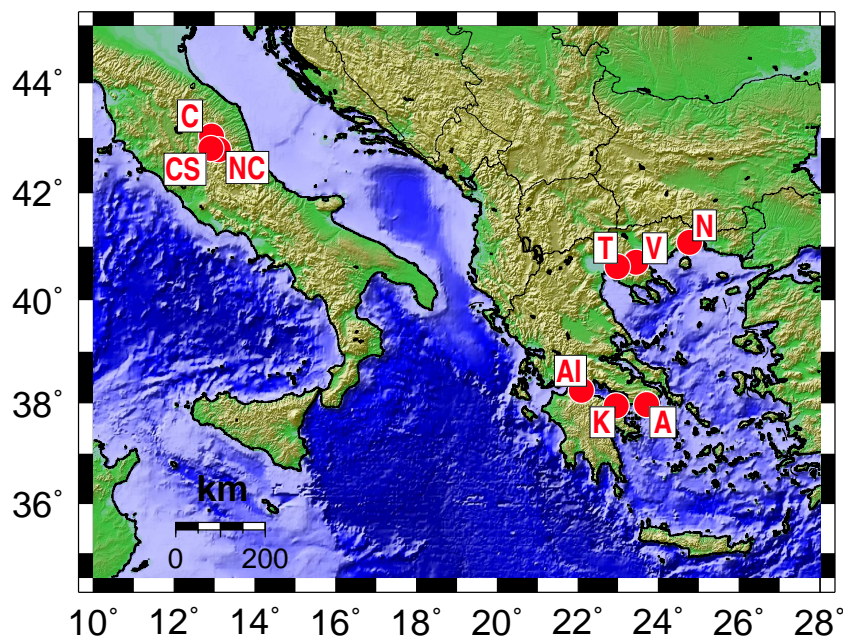


**Fig. 9** Location of the measurement sites where clear H/V peaks were observed. Additional information as well as full names are given in Tab. 2.

(lower part) gives the main characteristics of these sites and measurements. The NERIES measurements were performed in order to test the reliability and applicability of ambient vibration methods for site characterisation. Therefore, sites were selected for which velocity-depth profiles from boreholes, considered as ground-truth information for comparison, were available (Picozzi et al, 2007, N. Theodulidis, pers. comm., 2007). However, not all of the boreholes reached the bedrock. The site at Colfiorito is known to be non-one-dimensional, with a highly irregular sediment-bedrock interface (Di Giulio et al, 2003). This is readily apparent in the very different H/V peak frequencies measured at the two locations in Colfiorito (Tab. 2), even though the closest stations of the two SESAME arrays were only 165 m apart. As both locations were a notable distance from the borehole, the relevant structural information given by Di Giulio et al (2006) was utilised as reference in this case. The mean contrast of impedance,  $Z_m$ , between the sedimentary layers and the bedrock was calculated for the sites as described by Renalier et al (2009). A clear relationship between the observed H/V peak frequency,  $f_0$ , and the depth to the bedrock,  $d_{br}$ , on the one hand, and between the amplitude of the H/V peak,  $A_0$ , and  $Z_m$  on the other hand is not apparent for all of the sites. This is likely a result of the arrays being located significant distances from the boreholes, often 100 m or more (Renalier et al, 2009), for example because of the local topography, building structure, or admittance issues. Thus, lateral variation in either bedrock depth or sediment velocities, which is expected for example in Nestos, might already affect the comparison. Yet overall, with the exception of

Nestos, a general correlation is observed between the sites with the strongest impedance contrasts (strong impedance contrast sites as defined by Bonnefoy-Claudet et al, 2008,  $Z_m > 4.0$ ) and the largest peak amplitudes,  $A_0$ , measured. Similarly,  $f_0$  increases with decreasing bedrock depth, as expected, with the exception of the very slow site at Colfiorito (compare average velocity of the sediments,  $\bar{v}_s$ ). The dimension of the largest array deployment at each site is also provided to demonstrate the frequency resolution possible at each location.

The H/V results for the third deployment, array C (light grey in Fig. 10), for the site in Aigio differ from those of the other two, even though several station positions remained the same between arrays B and C. The measured H/V peaks are located at higher frequencies (6.2 Hz), with almost twice the amplitude. This variation is most likely due to a man-made source, as the spectra of array C show sharp peaks on the horizontal components at the respective frequency, which are not observed during the other two recordings. Hence, the H/V peaks of array C are considered not to result from site structure and disregarded in the analysis.

A detailed presentation of the results for two examples follows: Nestos, a rural site, which has a well-defined, large-amplitude H/V peak (Fig. 10h) and Athens, one of the most urban sites, which exhibits a broader peak of much lower amplitude that varies slightly with location (Fig. 10j)).

### 3.2.1 First example: Nestos

The measurement site is located near the construction site of a highway bridge across the Nestos River, north of its delta

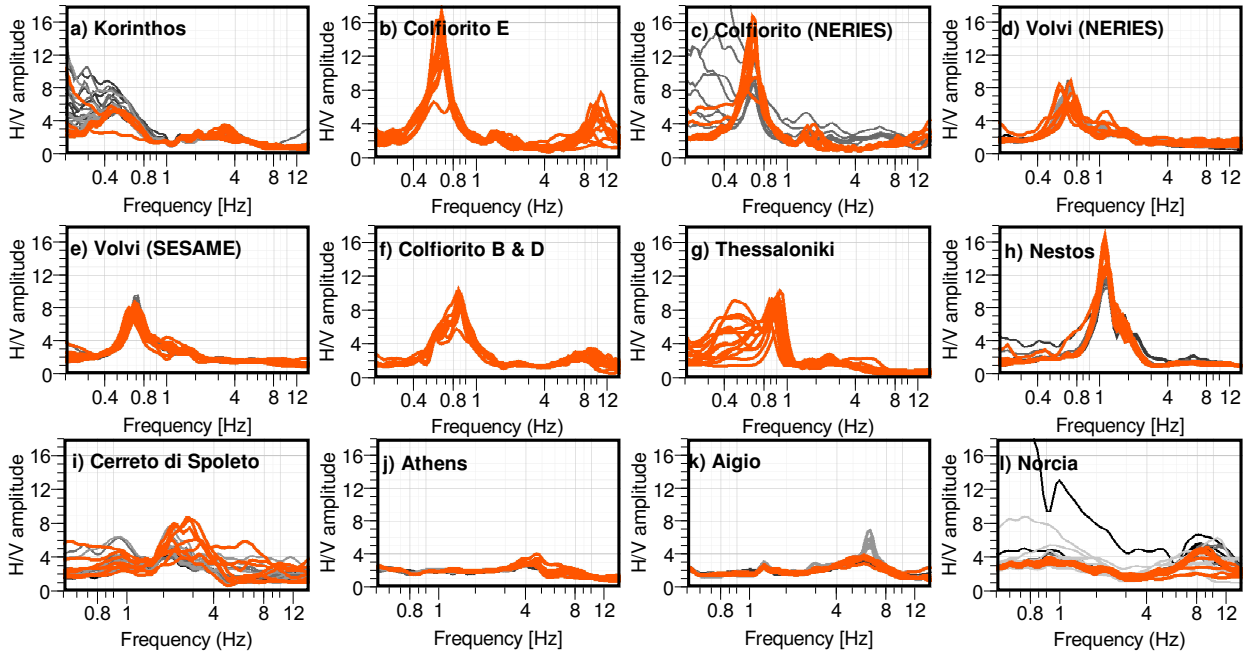


**Fig. 10** H/V curves measured at the individual sites, sorted by increasing H/V peak frequency. Orange colour refers to the curves measured at the array that is used for the analysis of polarisation vs. propagation direction at the H/V peak (with the exception of Norcia, this is the largest array), while thin lines in various shades of grey depict the curves measured with other (i.e. smaller) arrays at the same site. Note the different frequency axis used in i) to l).

in NE Greece. As expected near a large river, the site geology consists of fluvial deposits, which are poorly to moderately compacted, clean to silty sand, over weathered gneiss. Stratigraphy from five boreholes in the area reveals a number of lens-shaped inclusions and variable bedrock depths, with the depth of the sediment-bedrock interface increasing towards the river (Picozzi et al, 2007).

Investigation of the main propagation directions observed with the largest array shows a strong concentration around  $50^\circ$  to  $80^\circ$  for frequencies around 2 Hz, similar on all three components (Fig. 11). The horizontal polarisation analysis also reveals a pronounced maximum around 2 Hz for directions around  $155^\circ$  and a weaker concentration around  $325^\circ$  (Fig. 12). In both cases, the high-energy regions are more limited in frequency and broader in azimuth than in the synthetic cases, which can only be considered a coarse approximation of the real in-field situation. This implies that the FKPA method, which is based on a clear relationship between propagation and polarisation directions and problematic for completely random wavefields, might only be relevant for a narrower frequency band in this real-world example. Fig. 13 gives a more detailed picture of the distributions around 1.3 Hz, the peak frequency of the measured H/V curves. It shows a comparison of histograms for the propagation and polarisation directions over the five frequency bins centred at 1.3 Hz (1.22 to 1.40 Hz), similar to Fig. 6.

As already visible in the plots showing the main propagation and polarisation directions with frequency (Figs. 11 and 12), the main propagation directions (blue) are clustered around  $240^\circ$  and between  $30^\circ$  and  $70^\circ$  in this frequency range, while the polarisation directions (orange) strongly point to  $140^\circ$  to  $170^\circ$  and, to a lesser extent,  $320^\circ$  to  $350^\circ$ . Accordingly, there is a strong component with a  $90^\circ$  phase shift between the propagation and polarisation directions in the wavefield at frequencies around the H/V peak. The values of  $\alpha$  measured at the H/V peak by both FKPA and MSPAC can be found in Tab. 3. Both are comparatively low, below 40%, and agree within their uncertainties. Still, the value determined by MSPAC is larger than the one determined by FKPA, but also has a very large uncertainty. This might be because the H/V peak frequency of 1.3 Hz is associated with a strong decrease in  $\alpha$ , as determined by both methods (see Fig. 14). The  $\alpha$  values determined by MSPAC for the two neighbouring frequencies are 10% and 70%, respectively, with the value of 35% measured at 1.3 Hz located on the slope between them. Therefore, both methods indicate an increase in the Love wave contribution to the wavefield near the H/V peak. Fig. 14 reveals that FKPA results from different array sizes also agree well in the overlapping regions. One exception is the frequency band between 5 Hz and 7 Hz, covered by the intermediate and the smallest array. This discrepancy may be the result of variations in the sources that contribute

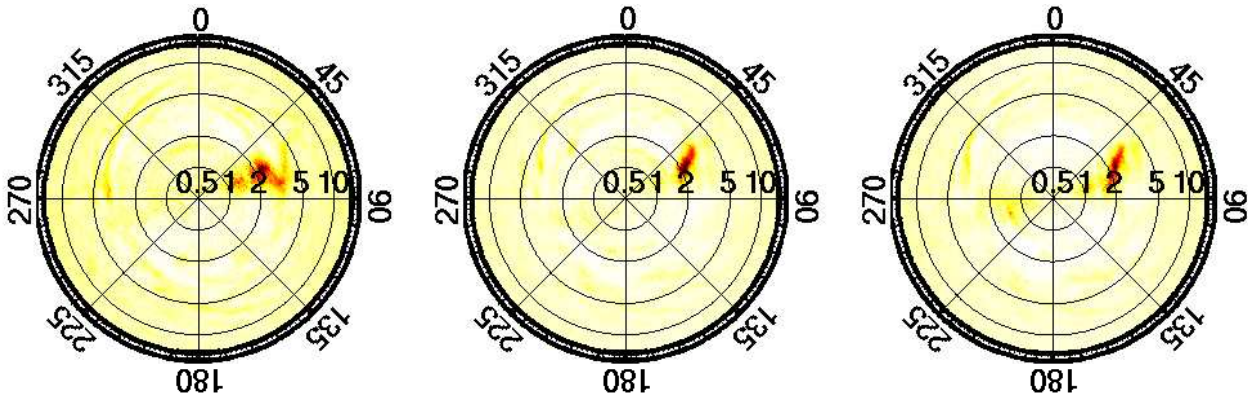


Fig. 11 Propagation directions observed in FK analysis of array C at Nestos, depicted as in Fig. 4, but for frequencies from 0.5 to 15 Hz. Left, center and right panel show results for vertical, east and north component, respectively.

to the frequency band between these two measurements. The estimates obtained with FKPA always lie within the error estimates from the values derived by MSPAC.

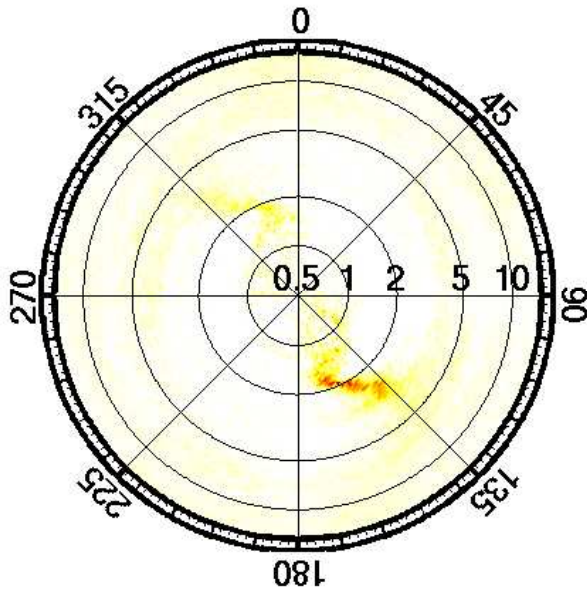


Fig. 12 Horizontal polarisation directions derived from analysis of the data recorded by array C at Nestos, displayed as in Fig. 4.

Tab. 4 lists the values for  $\alpha$  measured at the H/V peak frequency by FKPA, when each of the array stations are used individually, or the whole array is used together to estimate the horizontal polarisation direction. All of the values estimated using a single station are larger than the value derived using the whole array simultaneously. For most stations, the deviation is less than 10%, but two stations show a differ-

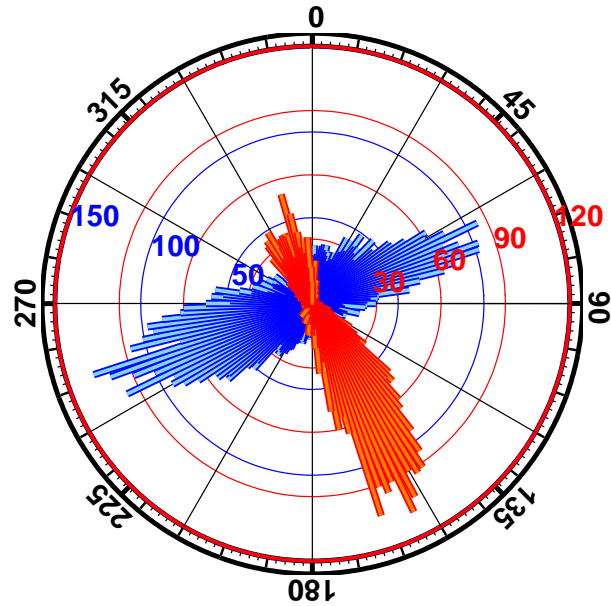
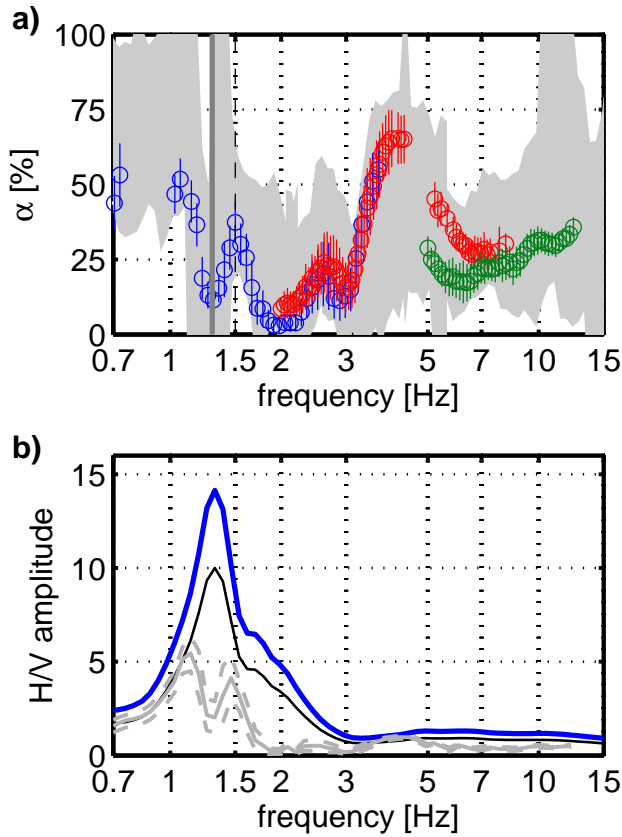


Fig. 13 Polarisation (orange) vs. propagation (blue) directions measured at array C in Nestos in the frequency band between 1.22 and 1.41 Hz, which encompasses the H/V peak at 1.3 Hz.

ence close to 20%. This result is unlike the observations from the synthetic cases, where single-station observations for the combined Love and Rayleigh wavefield do not exhibit such a large bias. But this can be thought of as the effect of uncertainty on the way  $\alpha$  is determined for a wavefield that is dominantly Love waves. In a distribution as imaged in Fig. 13, noisy data leads to a larger scatter in measured polarisation values. This in return, results in a randomly scattered contribution to the histograms of the angular shift between propagation and polarisation directions (compare Fig. 1), which increases the amplitude of the background level in the histograms. Scattering of values across the whole 360° of angular space tends to reduce the focusing of high am-



**Fig. 14** a) Distribution of measured values of  $\alpha$  with frequency at Nestos. Light grey shading fills standard deviation boundaries of the MSPAC results, while coloured circles with bars indicate results of FKPA analysis with standard deviations. The blue circles give results for the largest array while red circles outline measurement with the intermediate array and green circles those with the smallest array. The dark grey line marks the H/V peak frequency at 1.3 Hz, while thin dashed black line gives the theoretical lower resolution limit of the largest array. b) Average measured H/V curve for the largest array (blue) after correction for Love wave contribution as determined by FKPA (gray curve with standard deviations) and assuming a constant and equal contribution of Love and Rayleigh waves to the wavefield (black line).

plitudes around  $90^\circ$  or  $270^\circ$  and adds to the amplitudes observed around  $0^\circ$  and  $180^\circ$ , thus increasing the estimated amount of Rayleigh waves. This effect is not observed for the synthetic cases, as variations between different stations are not related to station quality (local level of disturbances close to the station or quality of the station installation, e.g., levelling, horizontal orientation, underground, shielding) in these cases, but only to the variations in the source wavefield. The results from the actual data seem to indicate that WAU04 and WAU05 are stations of below-average quality for this installation.

Finally, Fig. 14 b) shows the effect of correcting the measured H/V curves for the Love wave contribution as determined by FKPA. The correction significantly reduces the amplitudes of the curve, especially around the H/V peak.

**Table 3** Comparison of measured values for  $\alpha$ , using FKPA and MSPAC, at peak frequencies of the H/V curves show in Fig. 10. N or S behind the site name refers to NERIES and SESAME measurements, respectively. Measurements are sorted by increasing H/V peak frequency. For the long-term measurements at Colfiorito, results from afternoon time windows are listed to allow comparability with the NERIES measurement at the same site. For their temporal variability, see Tab. 5.

site	$f_0$ [Hz]	$\alpha_{FKPA}$ [%]	$\alpha_{MSPAC}$ [%]
Korinthos (N)	0.48	$44 \pm 10$	-
Colfiorito E (S)	0.65	$45 \pm 12$	-
Colfiorito (N)	0.65	$49 \pm 12$	-
Volvi (N)	0.7	$50 \pm 11$	-
Volvi (S)	0.7	$52 \pm 11$	-
Colfiorito B & D (S)	0.9	$42 \pm 6$	$15 \pm 22$
Thessaloniki (S)	1.0	-	-
Nestos (N)	1.3	$12 \pm 5$	$35 \pm 98$
Cerreto di Spoleto (N)	2.2	-	$50 \pm 60$
Athens C (N)	3.9	$31 \pm 5$	$15 \pm 25$
Athens D (N)	3.9	$31 \pm 4$	$30 \pm 25$
Aigio (N)	5.7	-	$30 \pm 39$
Norcia (N)	8.0	-	$40 \pm 38$

**Table 4** Estimates for  $\alpha$  in per cent at the H/V peak using single stations in polarisation analysis compared to the result when using the complete array for measurements at the two sites discussed in detail

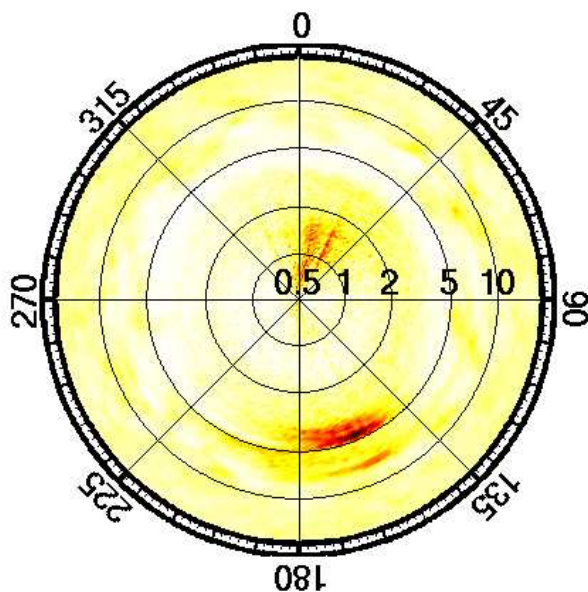
station	Nestos	Athens D
WAU01	$23 \pm 5$	$33 \pm 4$
WAU02	$17 \pm 4$	$36 \pm 4$
WAU03	$22 \pm 6$	$40 \pm 4$
WAU04	$35 \pm 6$	$42 \pm 5$
WAU05	$31 \pm 6$	-
WAU06	$17 \pm 5$	$38 \pm 4$
WAU07	$16 \pm 5$	$37 \pm 4$
WAU08	$14 \pm 4$	-
all	$12 \pm 5$	$31 \pm 4$

The narrow region of very low values of  $\alpha$  leads to a local minimum in the corrected H/V curve around 1.3 Hz and two smaller maxima on either side of it. In other words, the correction for the Love wave contribution alters the shape of the H/V curve for this case, similar to the synthetic example (Fig. 3), and shifts the peak frequency to a lower value around 1.1 Hz. The second maximum in the corrected curve can be related to a secondary maximum near 1.8 Hz in the H/V curves measured with the smaller arrays at this site but not resolved within the broader right flanks of the curves measured with the largest array (Fig. 10 h). Thus, the reason this secondary maximum is not always resolved might be a variation in the contribution of the Love waves to the wavefield at low frequencies for the different array deployments. As the frequency range discussed is covered only by the largest array in FKPA, this hypothesis can however not be investigated further with the data at hand. If the corrected H/V curve is then compared to the H/V curve calculated with the standard correction for equal Rayleigh and Love

1  
2  
3  
4  
5  
6 wave contents in the horizontal wavefield (black line), it re-  
7 veals there is a large difference between them. Amplitudes  
8 around the H/V peak are much higher when using the stan-  
9 dard correction, and no secondary maximum is resolved.

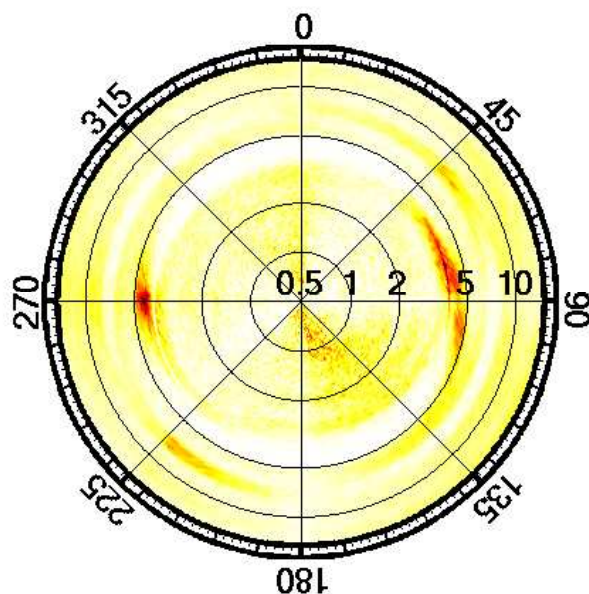
### 11 3.2.2 Second example: Athens

13 The measurement site is located on a yard of the Research  
14 Center for Public Works (K.E.D.E) in the Kalithea area, in  
15 the centre of the metropolitan region of greater Athens. The  
16 geological basement consists of the Athens schist series, cov-  
17 ered by fine-grained Quaternary deposits (Koukis and Sabatakis,  
18 2000). This series represents a flysch phase of delta-type de-  
19 posits of Upper Cretaceous age. These rocks have a variety  
20 of lithologies and are a very heterogeneous material with  
21 partly stiff, soil-like properties, which explains the rather  
22 low S-wave velocities around 800 m/s for the bedrock found  
23 in borehole logs. Isopachs for the sedimentary cover are over-  
24 all NNE-SSW, which is the direction of the Kifissos and Il-  
25 lisos rivers, on either side of the test site.



31  
32  
33  
34  
35  
36  
37  
38  
39  
40  
41  
42  
43  
44  
45  
46  
47  
48  
49  
50  
51  
52  
53  
54 **Fig. 15** Propagation directions observed as maximum concentration of  
55 sources in FK analysis of array D at Athens. Results are shown only for  
56 the east component, but look similar for vertical and north components  
57 as well as for data recorded with array C. Colour coding and frequency  
58 range depicted as in Fig. 4.

60 The propagation directions for the largest two arrays, C  
61 and D, which both have a good resolution at the respective  
62 frequencies, show a maximum at 135° to 180° around 4 Hz  
63 (Fig. 15) on all three components. The polarisation azimuths  
64  
65



59  
60  
61  
62  
63  
64  
65  
**Fig. 16** Horizontal polarisation directions derived from analysis of the  
data recorded by array D at Athens, displayed as in Fig. 4.

also show clear maxima around 4 Hz between 50° and 115°  
and, shifted by 180°, between 250° and 280° at both ar-  
rays (Fig. 16). Fig. 17 shows in more detail the azimuthal  
distributions around the H/V peak at 3.9 Hz, using the five  
frequency bins between 3.6 and 4.1 Hz and including data  
from the two horizontal components of both array C and D.  
As observed in Figs. 15 and 16, the propagation directions  
(blue) concentrate around an angle of 160°, while the po-  
larisation directions (orange) focus around 70°. In addition,  
angles between 240° and 270° are found. Again, the domi-  
nant component of the wavefield shows a 90° phase shift be-  
tween the propagation and polarisation direction at the H/V  
peak frequency. The values for  $\alpha$  at the H/V peak frequency  
determined with FKPA, as well as MSPAC, for both the ar-  
ray C and D data are listed in Tab. 3. Results from FKPA are

identical for both arrays, while results from MSPAC show some variability. But both methods do agree within their respective error margins. Measurements with the two arrays were performed in consecutive time windows (array C from approximately 12:35 pm local time to 01:25 pm, and array D from approximately 02:00 pm to 03:10 pm), and the FKPA result indicates an on average constant wavefield composition around the H/V peak, at least for the time span covered by these array recordings. An investigation across longer time spans is possible for the SESAME measurements at Colfiorito and discussed below.

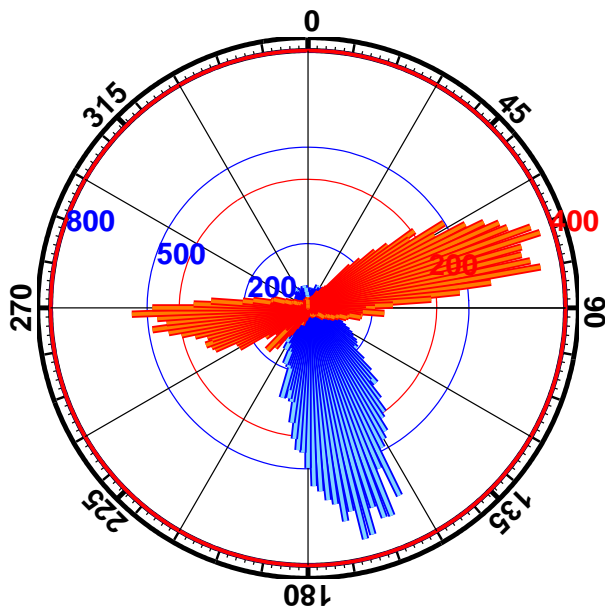


**Fig. 17** Polarisation (red) vs. propagation (blue) directions measured at arrays C and D in Athens in the frequency band between 3.6 and 4.15 Hz, which encompasses the H/V peak at 3.9 Hz.

Tab. 4 lists the values for  $\alpha$  measured at the H/V peak frequency by FKPA for array D, when each of the array stations are used individually, and as a whole, to estimate the horizontal polarisation direction. For array C, it was not possible to measure  $\alpha$  with the single station data, and values could only be derived at a few frequency points when using the whole array (Fig. 18 a)). Taken with the larger variability in the MSPAC results, this observation may indicate the results for array C are less certain than for array D. Again, single station estimates all produce larger values than using the complete array but are within 11% of the joint estimate. A possible explanation for this is given above in the discussion of the Nestos data set.

Fig. 18 a) shows the distribution of  $\alpha$  with frequency. Again, results from the different array sizes agree well within the overlapping region. Additionally, the estimates obtained always lie within the error estimates of the values derived by

MSPAC. However, it was not possible to derive any values for  $\alpha$  with FKPA from the data obtained with the smallest array, covering the highest frequencies. Correcting the measured H/V curve for the contribution of Love waves, determined by FKPA, again reduces the amplitude, especially around the H/V peak. This is also the main difference from the curve corrected assuming 50% of Love waves in the wavefield. In this case, the FKPA result is corroborated by the theoretical Rayleigh wave ellipticity calculated from the velocity model available from cross-hole measurements (Picozzi et al, 2007). The theoretical curve is overall a horizontal line with an amplitude of approximately 0.85, without a visible peak. Although the amplitude of the corrected curve is 1.0 rather than 0.85, it mimics the general character of the theoretical curve much more closely than the uncorrected, measured curve and the curve corrected for 50% Love waves.

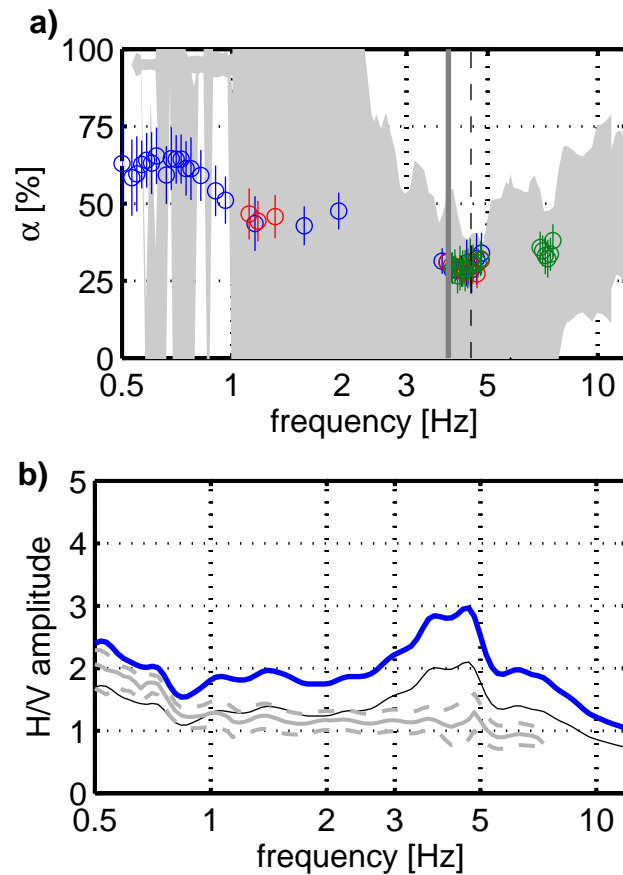


**Fig. 18** a) Distribution of measured values of  $\alpha$  with frequency at Athens, depicted as in Fig. 14. b) Average measured H/V curve for the largest array (blue) after correction for Love wave contribution as determined by FKPA (gray curve with standard deviations) and assuming a constant and equal contribution of Love and Rayleigh waves to the wavefield (black line).

**Table 5** Estimates for  $\alpha$  around the H/V peak (P) during different time windows recorded at Colfiorito. Note that H/V peak frequencies are different for arrays B & D (0.9 Hz) and E (0.65 Hz), respectively. For arrays B & D, estimates of  $\alpha$  at the trough frequency (T) of 1.9 Hz are also given. Time is given in local time, which is 2 hours in advance of GMT.

date	time	$\alpha_{B\&D}$ P [%]	$\alpha_E$ P [%]	$\alpha_{B\&D}$ T [%]
2002/07/29	15-16	$40 \pm 6$	-	$23 \pm 5$
	16-17	$37 \pm 6$	-	$26 \pm 6$
	17-18	-	-	$20 \pm 5$
2002/07/30	18-19	-	-	$17 \pm 5$
	19-20	$42 \pm 6$	$45 \pm 12$	$30 \pm 6$
	20-21	-	-	$31 \pm 6$
	21-22	-	$44 \pm 6$	$33 \pm 6$
	22-23	-	-	$37 \pm 7$
2002/07/31	23-24	$48 \pm 8$	$46 \pm 6$	$41 \pm 6$
	00-01	$43 \pm 8$	-	$37 \pm 6$
	01-02	-	$49 \pm 7$	$37 \pm 7$
	02-03	-	-	$37 \pm 9$
	03-04	$44 \pm 7$	$43 \pm 9$	$30 \pm 9$
	04-05	-	-	$25 \pm 9$
	05-06	$39 \pm 7$	-	$26 \pm 8$
06-07	$46 \pm 7$	$52 \pm 7$	$34 \pm 8$	
07-08	$35 \pm 6$	-	$26 \pm 9$	
08-09	$42 \pm 6$	-	$22 \pm 7$	

### 3.2.3 Temporal variations

For the Colfiorito site, measurements over a consecutive interval of 15 hours, with additional three hours of measurements on another day, were available from the SESAME campaign. FKPA analysis was applied individually to each hour of the recordings (Tab. 5). Unfortunately, because the H/V peaks are located near the limits of resolution for the arrays installed, measurements for all time intervals were not possible. However, a trough is consistently observed in the H/V recordings from arrays B & D at 1.9 Hz. At this frequency, measurements were possible during all time windows and hint at variations related to the time of day. In general, lower values for  $\alpha$  (less than 30%) are found during the afternoon and evening, from 03:00 pm to 08:00 pm. At night, the measured contribution of Rayleigh waves at this frequency increases, to more than 35%. After about 04:00 am, the values of  $\alpha$  are small again, generally around 25%, with exceptionally high values obtained between 06:00 am and 07:00 am. If this one hour is ignored, the maximum values for  $\alpha$  are also observed between 08:00 pm and 04:00 am in the limited data available for the H/V peaks. The values measured for arrays B & D and array E do not match exactly, as the H/V peaks are located at different frequencies (0.9 Hz vs. 0.65 Hz), but they are similar overall. The measured values of  $\alpha$  over the whole frequency range, as shown in Fig. 19 a) for three one-hour time intervals during afternoon, night, and morning, demonstrate that the temporal variation is observed over the frequency range from 1 Hz to 2.5 Hz. While the curves for afternoon (07:00-08:00 pm,

blue) and morning (07:00-08:00 am, green) are very consistent over the interval from 1.5 Hz and 2.5 Hz, the curve measured at night (01:00-02:00 am, red) shows higher values for  $\alpha$ . This is corroborated by MSPAC measurements, which exhibit a similar variation (Fig. 19 a)). However, for the frequency range between 1.0 Hz and 1.2 Hz, the curve measured in the morning (07:00-08:00 am, green) points to a higher percentage of Love waves. Indications of this variability also appear in the H/V curves averaged over the individual time intervals. The curve measured during the morning shows higher amplitudes between 1.0 Hz and 1.2 Hz, where lower values of  $\alpha$  were derived, while the curve measured at night shows lower amplitudes around 2 Hz, where higher values of  $\alpha$  were extracted. Nevertheless, the fluctuations in the average H/V curves are rather small and well within their individual standard deviations.

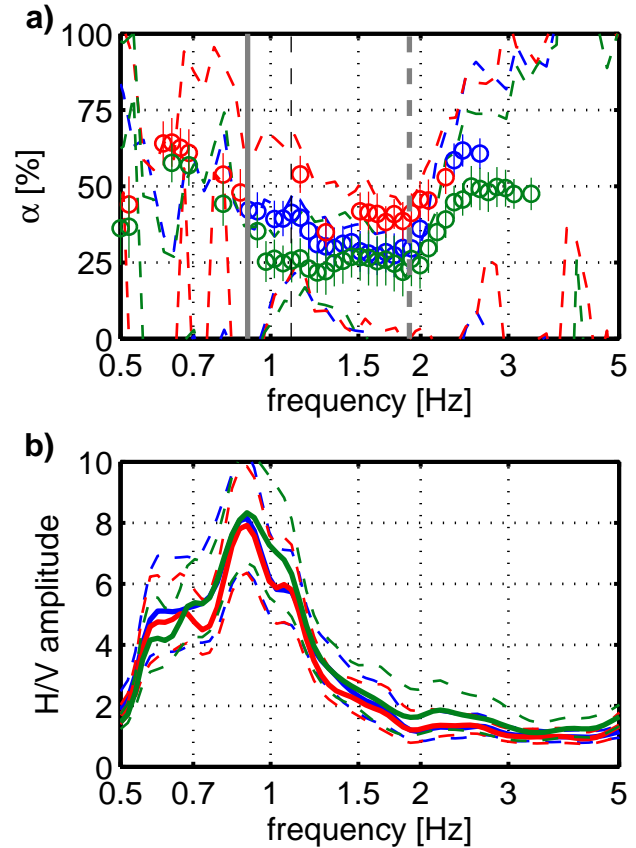


**Fig. 19** a) Distribution of measured values of  $\alpha$  with frequency at Colfiorito for SESAME arrays B and D, within three different time windows: 07:00-08:00 pm (blue), 01:00-02:00 am (red) and 07:00-08:00 am (green). Dashed lines outline the standard deviation boundaries of MSPAC results, while coloured circles with bars indicate results of FKPA with standard deviations. The solid grey line marks the H/V peak frequency at 0.9 Hz, while the dashed grey line locates the H/V trough frequency at 1.9 Hz. The dashed black line gives the theoretical lower resolution limit of the array. b) Average H/V curves measured during these time windows with standard deviations. The same colour coding as in a) is used.

A large amount of Love waves have been observed in data from Colfiorito valley before (Maresca et al, 2006). Di Giulio et al (2003) and Maresca et al (2006) proposed the Love waves are generated by diffraction at the sharp base-ment topography within the valley. The observations presented herein indicate that in addition, there are temporal variations in the sources responsible for the generation of at least some of the Love waves.

At other sites, only shorter time ranges were collected. For example, at Lefkos Pirgos, two consecutive hours of measurements can be compared and agree well (Fig. 20 f)). At the other NERIES sites, arrays of increasing size were deployed one after the other. The large overall overlap between measurements from different arrays, also points to the short-term temporal consistency herein. But these measurements were conducted only during the daytime, and thus they cannot be directly compared to the observations at Colfiorito.

### 3.2.4 Summary

For all sites, estimates of  $\alpha$  at the H/V peak frequency are listed in Tab. 3. At some sites, where the H/V peak is located at very low frequencies, it was impossible to determine  $\alpha$  with one or both of the methods due to a lack of resolution.

In the case of Aigio, measurements near the peak and trough frequencies with FKPA can only be made with the data from array C, which shows a strong H/V peak at 6.2 Hz due to a man-made source (Fig. 10). This peak is also clearly mirrored by a strong minimum in  $\alpha$  at the corresponding frequency (see Fig. 20g)), indicating that the man-made source produces mainly Love waves. As this man-made source biases the measurements near the H/V peak frequency for array C, no values are listed for Aigio in Tab. 3.

In addition to the H/V peaks, distinct troughs in the H/V curve were observed at some of the locations. The values of  $\alpha$  at the trough frequencies are given in Tab. 6 for these cases. All trough frequencies are approximately twice the respective H/V peak frequency, as observed by Konno and Ohmachi (1998). As described by Nakamura (2000), the H/V trough should be related to a maximum of energy on the vertical component, caused by the Rayleigh Airy phase. However, in contrast to the observations for the synthetic data, the values of  $\alpha$ , determined at the H/V trough frequency by both FKPA and MSPAC, do not show any significant increase compared to the values determined at the H/V peak frequency.

The distribution of  $\alpha$  with frequency is displayed in Fig. 20 for all sites not presented in detail before, including results from both MSPAC and FKPA. Norcia and Cerreto di Spoleto are excluded from this compilation, as the data sets recorded at these sites only allowed for measurements of  $\alpha$  at a few isolated frequencies with the proposed method.

**Table 6** Same as Tab. 3 for H/V trough frequencies.

site	f [Hz]	$\alpha_{FKPA}$ [%]	$\alpha_{MSPAC}$ [%]
Korinthos (N)	1.0	-	-
Colfiorito (N)	1.3	$25 \pm 13$	$15 \pm 21$
Colfiorito B & D (S)	1.9	$30 \pm 6$	$5 \pm 17$
Cerreto di Spoleto (N)	5.0	-	$25 \pm 30$
Aigio (N)	12.0	-	$32 \pm 37$

The data from the NERIES measurement at Colfiorito show a large scatter between both array deployments as well as between adjacent frequencies of the same deployment (Fig. 20 c)). During this measurement, problems with the horizontal components of the sensors occurred, which probably had an adverse effect on the FK, as well as the polarisation analysis part of the FKPA method. As such, the observations derived from this measurement, that  $\alpha$  is larger at the H/V peak frequency than at the H/V trough frequency and has very small values near the trough, are not robust.

## 4 Discussion and Conclusions

Tests with synthetic datasets indicate that, at least above the lower limit of array resolution, which is around 4 Hz for the test dataset,  $\alpha$  can be determined in a consistent fashion by FKPA. Errors are less than 10%, even for cases that include higher modes or more than one distinct source region. However, in a truly random wavefield, the applicability of FKPA is limited as FK, as well as polarisation analysis, work best for a single dominant source active at a single time. In this instance, MSPAC can potentially complement the method as it basically assumes randomly distributed sources. However, in the synthetic tests, FKPA worked better than MSPAC for multi-modal wavefields. Furthermore, in the synthetic cases, FKPA and MSPAC estimates show an overlap in their standard deviations, but the MSPAC estimate at the H/V peak is somewhat larger. Overall, the general shape of the distribution of  $\alpha$  with frequency agrees for both methods.

When applied to real data, estimates from both methods generally also agree well. When deviations do occur, they do not show a systematic pattern, i.e., for Nestos, the MSPAC estimate is larger but for array C in Athens, the value derived by FKPA is larger. This observation argues against a systematic bias between the two methods, although the data available for comparison is limited. The case with the strongest discrepancy, i.e., the average result from FKPA is not within the standard deviation boundaries of MSPAC, although the error margins of both still overlap, is the case for the measurements at Colfiorito with arrays B & D of the SESAME campaign.

Towards low frequencies, where resolution of the arrays is lost, values of  $\alpha$  determined by MSPAC often approach 100% (e.g., Figs. 20 c), d), e), f)), while values determined

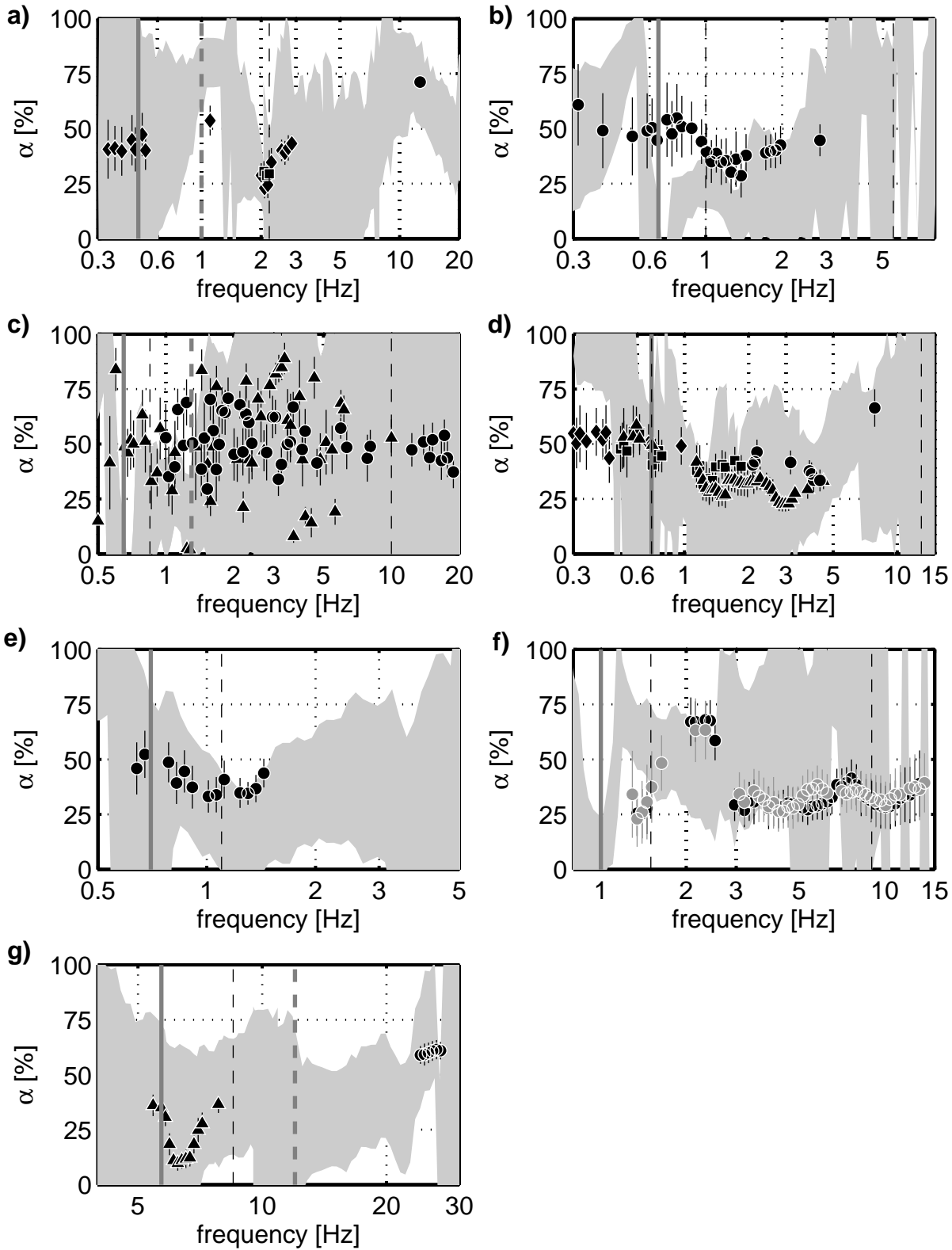


**Fig. 20** Distribution of measured values of  $\alpha$  with frequency for the sites a) Korinthos, b) Colfiorito E (SESAME), c) Colfiorito (NERIES), d) Volvi (NERIES), e) Volvi (SESAME), f) Thessaloniki, g) Aigio. The black symbols with bars indicate results of FKPA with standard deviations; different symbols refer to arrays of different sizes deployed at the same location (diamonds, triangles, squares and circles from largest to smallest, respectively). Light grey shading fills standard deviation boundaries of the MSPAC results. The dark grey solid lines marks H/V peak frequency and the dark grey dashed lines H/V trough frequency, where observable. The thin dashed black lines outline the theoretical lower (and, when located within the displayed frequency range, upper) resolution limits of the largest (and smallest, respectively) array at each site. For Thessaloniki, black and dark grey circles indicate measurements conducted during two consecutive hours of the early afternoon.

by FKPA in some cases seem to level off around 50% (Figs. 14 and 20 a, d). These observations likely show the different effects of lost resolution on the two methods. At two of the sites investigated, measurements with FKPA were only possible at some isolated, scattered frequency points. Judging from the synthetic tests, the reason probably is related to the absence of isolated, strong source regions, and the existence of a more random wavefield. In the case of Cerreto di Spoleto, one might propose that this could be due to a small mountain stream running directly next to (and, in the case of the largest deployment, even right through) the arrays. The running water acts more like a line source of ambient vibrations than a point source, besides being very close to the array, and thus violates the assumptions upon which the FK analysis is based. For the site of Norcia, the sources dominating the ambient vibration wavefield are less obvious. However, the results for both these sites clearly illustrate the limits of the proposed method.

Around the H/V peak, the values of  $\alpha$  derived from the FKPA measurements are in most cases between 40% and 52%, and they are in broad agreement with the MSPAC results. This indicates that the values of  $\alpha$  generally used to correct for the Love wave contribution to H/V curves (e.g. Konno and Ohmachi, 1998; Fäh et al, 2001; Arai and Tokimatsu, 2004; Castellaro and Mulargia, 2009) would not be too inaccurate in these cases. However, at several sites, the value of  $\alpha$  shows strong variation with frequency that are usually not considered in the standard corrections (e.g., Figs. 14 and 19). Besides, indications of temporal variations in  $\alpha$  have been found in measurements that cover 15 hours.

Furthermore, within the measurements considered, there are at least two datasets, which significantly deviate from the assumption of equal Love and Rayleigh wave contributions to the horizontal wavefield, Nestos and Athens (Fig. 14 and 18). In both cases, the H/V peak frequency is located close to a minimum in the distribution of  $\alpha$ . From a geological point of view, the two sites are both located on fluvial sediments, close to the mouths of the depositing rivers. It is interesting to note that none of the other sites studied herein share a similar geological setting. When considering the site characteristics in more detail, though (Tab. 2), differences are clear. Nestos is a high-impedance contrast site with an intermediate bedrock depth, while Athens is a shallow, low-impedance contrast site with on average faster sediment velocities. These differences are also mirrored in the observed resonance frequencies and amplitudes (Tab. 2). For high-impedance contrast sites, it has been suggested from modelling that the Love wave Airy phase can significantly influence, and might even dominate, the wavefield around the H/V peak (Bonney-Claudet et al, 2008). However, for a low-impedance contrast site, this result is surprising. In addition, sources contributing to the noise wavefield are also expected to differ because the site in Athens is in a very ur-

ban location, while the site at Nestos is situated in a more rural environment.

Accordingly, as both of the sites presented in detail herein show different characteristics, no general rule for the existence of a large Love wave contribution to the wavefield around the H/V peak can be derived from a priori site information, especially when temporal variations also need to be considered. This, in return, implies that additional array measurements to characterise the horizontal wavefield are always useful to validate, or reject, the assumption of an equal, and frequency-independent, Love and Rayleigh wave content when correcting H/V amplitudes.

**Acknowledgements** This research was funded by the EC within research programm NERIES, JRA4. The author further wants to thank M. Ohrmberger for help with the calculation of synthetic noise data sets and helpful discussions and A. Köhler for aid with the MSPAC analysis. I am grateful to M. Knapmeyer for reviewing earlier versions of this draft and profitable advice. Two anonymous reviewers provided constructive comments and suggestions that helped to improve the manuscript substantially.

## References

- Aki K (1957) Space and time spectra of stationary stochastic waves, with special reference to microtremors. *Bull Earthq Res Inst* 35:415–457
- Alfaro A, Pujades LG, Goula X, Susagna T, Navarro M, Sánchez J, Canas JA (2001) Preliminary map of soil's predominant periods in Barcelona using microtremors. *Pure Appl Geophys* 158:2499–2511
- Anastasiadis A, Raptakis D, Pitilakis K (2001) Thessaloniki's detailed microzoning: surface structure as basis for site response analysis. *Pure appl geophys* 158:2597–2633
- Arai H, Tokimatsu K (2004) S-wave velocity profiling by inversion of microtremor H/V spectrum. *Bull Seism Soc Am* 94(1):53–63
- Arai H, Tokimatsu K (2005) S-wave velocity profiling by joint inversion of microtremor dispersion curve and horizontal-to-vertical (H/V) spectrum. *Bull Seism Soc Am* 95(5):1766–1778
- Arai H, Tokimatsu K (2008) Three-dimensional  $v_s$  profiling using microtremors in Kushiro, Japan. *Earthq Eng Struct Dyn* 37:845–859, doi:10.1002/eqe.788
- Athanasopoulos GA, Pelekis PC, Leonidou EA (1999) Effects of surface topography on seismic ground response in the Egion (Greece) 15 June 1995 earthquake. *Soil Dyn Earthq Eng* 18(2):135–149
- van der Baan M (2009) The origin of SH-wave resonance frequencies in sedimentary layers. *Geophys J Int* 178:1587–1596, doi:10.1111/j.1365-246X.2009.04245.x
- Bonney-Claudet S, Cornou C, Bard PY, Cotton F, Moczo P, Kristek J, Fäh D (2006a) H/V ratio: a tool for

- site effects evaluation. Results from 1-D noise simulations. *Geophys J Int* 167:827–837, doi:10.1111/j.1365-246X.2006.03154.x
- Bonnefoy-Claudet S, Cotton F, Bard PY (2006b) The nature of noise wavefield and its application for site effects studies A literature review. *Earth-Science Reviews* 79:205–227, doi:10.1016/j.earscirev.2006.07.004
- Bonnefoy-Claudet S, Köhler A, Cornou C, Wathelet M, Bard PY (2008) Effects of Love waves on microtremor H/V ratio. *Bull Seism Soc Am* 98(1):288–300, doi:10.1785/0120070063
- Bonnefoy-Claudet S, Baize S, Bonilla LF, Berge-Thierry C, Pasten C, Campos J, Volant P, Verdugo R (2009) Site effect estimation in the basin of Santiago de Chile using ambient noise measurements. *Geophys J Int* 176:925–937, doi:10.1111/j.1365-246X.2008.04020.x
- Bragato PL, Laurenzano G, Barnaba C (2007) Automatic zonation of urban areas based on the similarity of H/V spectral ratios. *Bull Seism Soc Am* 97(5):1404–1412, doi:10.1785/0120060260
- Cara F, Cultrera G, Azzara RM, De Rubeis V, Di Giulio G, Giammarinaro MS, Tosi P, Vallone P, Rovelli A (2008) Microtremor measurement in the city of Palermo, Italy: Analysis of the correlation between geology and damage. *Bull Seism Soc Am* 98(3):1354–1372, doi:10.1785/0120060260
- Castellaro S, Mulargia F (2009)  $V_{S30}$  estimates using constrained H/V measurements. *Bull Seism Soc Am* 99(2A):761–773, doi:10.1785/0120080179
- D’Amico V, Picozzi M, Baliva F, Albarello D (2008) Ambient noise measurements for preliminary site-effects characterization in the urban area of Florence, Italy. *Bull Seism Soc Am* 98(3):1373–1388, doi:10.1785/0120070231
- Di Giulio G, Rovelli A, Cara F, Azzara RM, Marra F, Basili R, Caserta A (2003) Long-duration asynchronous ground motions in the Colfiorito plain, central Italy, observed on a two-dimensional dense array. *J Geophys Res* 118(B10):2486, doi:10.1029/2002JB002367
- Di Giulio G, Cornou C, Ohrnberger M, Wathelet M, Rovelli A (2006) Deriving wavefield characteristics and shear-velocity profiles from two-dimensional small-aperture array analysis of ambient vibrations in a small-size alluvial basin, Colfiorito, Italy. *Bull Seism Soc Am* 96(5):1915–1933, doi:10.1785/0120060119
- Dravinski M, Ding G, Wen KL (1996) Analysis of spectral ratios for estimating ground motion in deep basins. *Bull Seism Soc Am* 86(3):646–654
- Duval AM, Vidal S, Méneroud JP, Singer A, De Santis F, Ramos C, Romero G, Rodriguez R, Pernia A, Reyes N, Grimán C (2001) Caracas, Venezuela, site effect determination with microtremors. *Pure Appl Geophys* 158:2513–2523
- Endrun B, Renalier F (2008) Report on in-situ measurements at the 20 selected sites. Deliverable D2, NERIES-Project JRA4 Task C, EU-FP6 EC project number 026130, [http://www.neries-eu.org/main.php/JRA4\\_D2\\_main\\_appendix1\\_appendix2.pdf?fileitem=130253](http://www.neries-eu.org/main.php/JRA4_D2_main_appendix1_appendix2.pdf?fileitem=130253)
- Endrun B, Ohrnberger M, Savvaidis A (2009) On the repeatability and consistency of ambient vibration array measurements. *Bull Earthq Eng* doi:10.1007/s10518-009-9159-9
- Fäh D, Rüttner E, Noack F, Kruspan P (1997) Microzonation of the city of Basel. *J Seism* 1:87–102
- Fäh D, Kind F, Giardina D (2001) A theoretical investigation of average H/V ratios. *Geophys J Int* 145:535–549
- Fäh D, Kind F, Giardini D (2003) Inversion of local S-wave velocity structures from average H/V ratios, and their use for the estimation of site-effects. *J Seism* 7:449–467
- Garcia-Jerez A, Navarro M, Alcalá FJ, Luzón F, Pérez-Ruiz JA, Enomoto T, Vidal F, Ocaña E (2007) Shallow velocity structure using joint inversion of array and h/v spectral ratio of ambient noise: the case of Mula town (SE of Spain). *Soil Dyn Earthq Eng* 27(10):907–919, doi:10.1016/j.soildyn.2007.03.001
- Guillier B, Atakan K, Chatelain JL, Havskov J, Ohrnberger M, Cara F, Duval AM, Zacharopoulos S, Teves-Costa P, the SESAME Team (2008) Influence of instruments on the H/V spectral ratios of ambient vibrations. *Bull Earthq Eng* 6:3–32, doi:10.1007/s10518-007-9039-0
- Herrmann RB (2001) Computer programs in seismology. Tech. Rep. Version 3.1, St. Louis University
- Hobiger M, Bard PY, Cornou C, Le Bihan N (2009) Single station determination of Rayleigh wave ellipticity by using the random decrement technique (RayDec). *Geophys Res Lett* 34:L14,303, doi:10.1029/2009GL038863
- Jurkevics A (1988) Polarization analysis of three-component array data. *Bull Seism Soc Am* 78(5):1725–1743
- Köhler A, Ohrnberger M, Scherbaum F, Wathelet M, Cornou C (2007) Assessing the reliability of the modified three-component spatial autocorrelation technique. *Geophys J Int* 168:779–796, doi:10.1111/j.1365-246X.2006.03253.x
- Konno K, Ohmachi T (1998) Ground-motion characteristics estimated from spectral ratio between horizontal and vertical components of microtremors. *Bull Seism Soc Am* 88(1):288–241
- Koukis G, Sabatakis N (2000) Engineering geological environment of Athens, Greece. *Bull Eng Geol Env* 59:127–135
- Lachet C, Bard PY (1994) Numerical and theoretical investigations on the possibilities and limitations of Nakamura’s technique. *J Phys Earth* 42:377–397
- Lacoss RT, Kelly EJ, Toksöz MN (1969) Estimation of seismic noise structure using arrays. *Geophysics* 34:21–38

- Langston CA, Chiu SCC, Lawrence Z, Bodin P, Horton S (2009) Array observations of microseismic noise and the nature of H/V in the Mississippi embayment. *Bull Seism Soc Am* 99(5):2893–2911, doi:10.1785/0120080189
- LeBrun B, Hatzfeld D, Bard PY (2001) Site effect study in urban area: Experimental results in Grenoble (France). *Pure Appl Geophys* 158:2543–2557
- Lermo J, Chávez-García FJ (1994) Are microtremors useful in site response evaluation? *Bull Seism Soc Am* 84(5):1350–1364
- Lunedei E, Albarello D (2009) On the seismic noise wavefield in a weakly dissipative layered Earth. *Geophys J Int* 177:1001–1014, doi:10.1111/j.1365-246X.2008.04062.x
- Malischewsky PG, Scherbaum F (2004) Love's formula and H/V-ratio (ellipticity) of Rayleigh waves. *Wave Motion* 40:57–67, doi:10.1016/j.wavemoti.2003.12.015
- Maresca R, Galluzzo D, Del Pezzo E (2006) H/V spectral ratios and array techniques applied to ambient noise recorded in the Colfiorito Basin, Central Italy. *Bull Seism Soc Am* 96(2):490–505, doi:10.1785/0120050057
- Nagashima E, Maeda T (2005) Inversion analysis on surface wave dispersion curves and H/V spectra by neighbourhood algorithm. In: 6th World Congress of Structural and Multidisciplinary Optimization, Rio de Janeiro, Brazil
- Nakamura Y (1989) A method for dynamic characteristics estimation of subsurface using microtremor on the ground surface. *Q Rept Railway Tech Res Inst* 30(1):25–33
- Nakamura Y (2000) Clear identification of fundamental idea of Nakamura's technique and its applications. In: Proceedings of the 12th World Conference on Earthquake Engineering, Auckland, New Zealand
- Nogoshi M, Igarashi T (1971) On the amplitude characteristics of microtremor (part 2). *J Seismol Soc Japan* 24:26–40, (in Japanese with English abstract)
- Ohrnberger M, Vollmer D, Scherbaum F (2006) WARAN - a mobile wireless array analysis system for in-field ambient vibration dispersion curve estimation. In: First European Conference on Earthquake Engineering and Seismology, Geneva, Switzerland, paper 2017, p 284, [http://www.ecees.org/abstract\\_book.pdf](http://www.ecees.org/abstract_book.pdf)
- Okada H (2003) The microtremor survey method, *Geophysical Monograph Series*, vol 12. Society of Exploration Geophysicists
- Panou AA, Theodulidis N, Hatzidimitriou P, Stylianidis K, Papazachos CB (2005a) Ambient noise horizontal-to-vertical spectral ratio in site effects estimation and correlation with seismic damage distribution in urban environment: the case of the city of Thessaloniki(Northern Greece). *Soil Dyn Earthq Eng* 25(4):261–274, doi:10.1016/j.soildyn.2005.02.004
- Panou AA, Theodulidis NP, Hatzidimitriou PM, Savvaidis AS, Papazachos CB (2005b) Reliability of ambient noise horizontal-to-vertical spectral ratio in urban environments: the case of Thessaloniki City (Northern Greece). *Pure appl Geophys* 162:891–912, doi:10.1007/s00024-004-2647-6
- Parolai S, Picozzi M, Richwalski SM, Milkereit C (2005) Joint inversion of phase velocity dispersion and H/V ratio curves from seismic noise recordings using a genetic algorithm, considering higher modes. *Geophys Res Lett* 32:L01,303, doi:10.1029/2004GL021115
- Picozzi M, Albarello D (2007) Combining genetic and linearized algorithms for a two-step joint inversion of Rayleigh wave dispersion and H/V spectral ratio curves. *Geophys J Int* 169:189–200, doi:10.1111/j.1365-246X.2006.03282.x
- Picozzi M, Sabetta F, Theodulidis N, Zacharopoulos S, Savvaidis A, Bard PY, Cornou C, Gueguen P, Fäh D, Kalogeras I, Akkar S, Rinaldis D, Tanircan G (2007) Selected sites and available information. Deliverable D1, NERIES-Project JRA4 Task C, EU-FP6 EC project number 026130, <http://www.neries-eu.org/main.php/JRA4-D1-Task%20A.pdf?fileitem=13025315>
- Picozzi M, Strollo A, Parolai S, Durukai E, Özel O, Karabulut S, Zschau J, Erdik M (2009) Site characterization by seismic noise in Istanbul, Turkey. *Soil Dyn Earthq Eng* 29(3):469–482, doi:10.1016/j.soildyn.2008.05.007
- Poggi V, Fäh D (2009) Estimating Rayleigh wave particle motion from three-component array analysis of ambient vibrations. *Geophys J Int* doi:10.1111/j.1365-246X.2009.04402.x
- Raptakis D, Chavez-Garcia FJ, Makra K, Pitalakis K (2000) Site effects at Euroseistest - I. Determination of the valley structure and confrontation of observations with 1D analysis. *Soil Dyn Earthq Eng* 19:1–22
- Renalier F, Jongmans D, Savvaidis A, Wathelet M, Endrun B, Cornou C (2009) Influence of parameterisation on inversion of surface wave dispersion curves and definition of an inversion strategy for sites with a strong Vs contrast. submitted to *Geophysics*
- Satoh T, Kawase H, Iwata T, Higashi S, Sato T, Irikura K, Huang HC (2001) S-wave velocity structure of the Taichung basin, Taiwan, estimated from array and single-station records of microtremors. *Bull Seism Soc Am* 91(5):1267–1282
- Scherbaum F, Hinzen KG, Ohrnberger M (2003) Determination of shallow shear wave velocity profiles in the Cologne,Germany area using ambient vibrations. *Geophys J Int* 152:597–612
- SESAME (2002) Report on the array data set for different sites - WP05 instrumental layout for array measurements. Deliverable D06.05, University of Potsdam, Germany, [http://sesame-fp5.obs.ujf-grenoble.fr/Delivrables/D06-05\\_Texte.pdf](http://sesame-fp5.obs.ujf-grenoble.fr/Delivrables/D06-05_Texte.pdf)
- SESAME (2005a) Guidelines for the implementation of the H/V spectral ratio technique on ambient

- 1  
2  
3  
4  
5  
6 vibration measurements and interpretation. Deliverable D23.12, University of Potsdam, Germany,  
7 <http://sesame-fp5.obs.ujf-grenoble.fr/Delivrables/Del->  
8 [D23-HV\\_User\\_Guidelines.pdf](http://sesame-fp5.obs.ujf-grenoble.fr/Delivrables/Del-D23-HV_User_Guidelines.pdf)  
9
- 10 SESAME (2005b) Recommendations for quality array  
11 measurements and processing. Deliverable D24.13,  
12 <http://sesame-fp5.obs.ujf-grenoble.fr/Delivrables/Del->  
13 [D24-Wp13.pdf](http://sesame-fp5.obs.ujf-grenoble.fr/Delivrables/Del-D24-Wp13.pdf)  
14
- 15 Souriau A, Roullé A, Ponsolles C (2007) Site effects in the  
16 city of Lourdes, France, from H/V measurements: Impli-  
17 cations for seismic-risk evaluation. *Bull Seism Soc Am*  
18 79(6):2118–2136, doi:10.1785/0120060224
- 19 Tokeshi JC, Sugimura Y, Karkee MB (2000) Parametric  
20 study on simulated microtremors and its application to in-  
21 terpretation of microtremor records. *J Struct Constr Eng,*  
22 *AIJ* 535:69–78
- 23 Tuladhar R, Yamazaki F, Warnitchai P, Saita J (2004) Seis-  
24 mic microzonation of the greater Bangkok area using mi-  
25 crotremor observations. *Earthq Eng Struct Dyn* 33:211–  
26 225, doi:10.1002/eqe.345
- 27 Wathelet M (2005) Array recordings of ambient vibra-  
28 tions: surface-wave inversion. Phd thesis, Université de  
29 Liège, Faculté des Sciences Appliquées, available online  
30 at <http://marc.geopsy.org/publi/these.pdf.gz>  
31
- 32 Wathelet M, Jongmans D, Ohrnberger M, Bonnefoy-Claudet  
33 S (2008) Array performance for ambient vibrations on a  
34 shallow structure and consequences over  $v_s$  inversion. *J*  
35 *Seism* 12:1–19, doi:10.1007/s10950-007-9067-x
- 36 Yamanaka H, Takemura M, Ishida H, Niwa M (1994) Char-  
37 acteristics of long-period microtremors and their appli-  
38 cability in exploration of deep sedimentary layers. *Bull*  
39 *Seism Soc Am* 84(6):1831–1841  
40  
41  
42  
43  
44  
45  
46  
47  
48  
49  
50  
51  
52  
53  
54  
55  
56  
57  
58  
59  
60  
61  
62  
63  
64  
65

## Response to review JOSE405 - "Love wave contribution to the ambient vibration H/V amplitude peak observed with array measurements" by B. Endrun

Dear Editor,

in response to my submission of the manuscript, I received two constructive and detailed reviews. When producing the revised version of the manuscript, I considered all the points raised by the reviewers and improved the paper accordingly.

When working on the revision, it turned out that, due to the use of different versions of the geopsy software, H/V curves from the actual data were calculated in an inconsistent way. Now, the vector addition yielding total horizontal energy is used for all sites, and the synthetic data. This not only provides consistency, but furthermore is the correct way to calculate H/V curves when attempting to correct them for the Love wave content of the wavefield. This change increased the amplitudes of the curves measured at all Italian sites as well as Thessaloniki, and the curves derived from the synthetic datasets, by a factor of  $\sqrt{2}$ . However, this does neither affect the determination of  $\alpha$  nor the details of the presented method and the conclusions drawn.

In addition, two changes in data processing were incorporated into the revision. Firstly, only data of the horizontal components are used for the FK analysis to measure propagation directions now. The reasoning behind this change is that to correct for the Love wave contribution to the horizontal components of the wavefield, the estimate of  $\alpha$  should also be derived from these components only. As also stated in the original version of the text, including or ignoring the vertical component in the calculations does not change the results in any distinct way. Secondly, during the revision I realised that the  $360^\circ$  periodicity in the distributions of angular shifts between propagation and polarisation directions was handled incorrectly in the original submission (visible in the way Fig. 1 changed). I corrected this error, which resulted in slightly different choices of the threshold parameters used in the calculations. However, the resulting values for  $\alpha$  proved to be rather stable with regard to these changes. Although actual values derived for  $\alpha$  may have changed by a small amount, the overall trend of the results is robust and the conclusions drawn are not affected by the corrections described above.

One substantial issue raised by Reviewer #1 is the English level of the manuscript. As native speakers are few and hard to come by at our institute, we decided to employ a professional editing and proofreading service to revise the language of the document (excluding figure and table captions; see attached certificate from American Journal Experts). I hope and trust that it is more pleasant to read and easier accessible now.

In the following, I address and reply to all comments by both reviewers.

## Reviewer #1

### Global comments

However, the English level needs to be addressed seriously, for the whole document and especially for Sections 1 and 2. While the ideas developed in the document are worth publishing, the reading of the document is very unpleasant and makes it quite difficult to understand. This is a serious issue to revise to improve the manuscript. I would suggest you use help from a native English speaker in order to improve the document.

See above (and attached certificate from American Journal Experts); I hope the revision of the language by a professional service sufficiently improved the flow of the text and the phrasing.

In the revised version, please indicate the exact location of all Figures and Tables in the text. Figures and Tables are inserted at their correct places in the text.

You conclude that the corrections applied to H/V curves are generally made without taking into account the strong variations of  $\alpha$  with frequency, for which you develop a methodology to estimate. It would be important to demonstrate how your methodology helps better estimating the corrected H/V curves on H/V field observations. You present in Figure 3 the H/V curve corrected for the proportion of Love waves for synthetic cases. Why don't you present the same for H/V observations in Nestos and Athens, or any other cases presented in Figure 9? It would strengthen your conclusions about the use of your methodology by validating its application on field data.

I added Figs. 14 and 18 address this issue. Parts b) of these figures show average H/V curves measured with the largest arrays at Nestos (Fig. 14) and Athens (Fig. 18) before and after correcting for the contribution of Love waves to the wavefield as determined by FKPA. For comparison, the results of correcting with a constant factor of 50% Love waves, as often assumed in the literature, are also shown. These figures clearly depict the difference between using a constant factor or the frequency-dependent estimate of  $\alpha$  from the data itself for correction. As a large contribution of Love waves to the H/V peak was found for both of these sites, the amplitudes of the curves are significantly reduced when taking into account the actual measured values of  $\alpha$ . For the site in Athens, where this comparison is possible, the H/V curve corrected with measured values of  $\alpha$  shows a better agreement to the curve predicted from borehole data than both the original data and the curve corrected with a constant factor of 50%. This is an encouraging result in favour of the proposed methodology.

The conclusions you made in the 2nd last paragraph of the manuscript are very important

concerning the potential and limits of the methodology you developed. You then state, in the last paragraph of the manuscript, that you can never be sure about the validity of the assumption of equal Love and Rayleigh waves. It leaves the reader with a negative conclusion on the initial state of the problem (using equal Love and Rayleigh), and with the impression you don't really conclude on the advantages of using the methodology you just developed. It might just be a matter of reshuffling the last two paragraphs of the text, or adding one last sentence to conclude on your methodology.

I rewrote the last paragraph, to state explicitly that without any additional measurements (array measurements like FKPA or MSPAC as used in the manuscript or potentially also single-station measurements of the wavefield content), one cannot be sure about the assumption of equal Love and Rayleigh wave contribution to the ambient vibrations. It more clearly points out the benefits of the method developed in this paper now:

*Accordingly, as both of the sites presented in detail herein show different characteristics, no general rule for the existence of a large Love wave contribution to the wavefield around the H/V peak can be derived from a priori site information, especially when temporal variations also need to be considered. This, in return, implies that additional array measurements to characterise the horizontal wavefield are always useful to validate, or reject, the assumption of an equal, and frequency-independent, Love and Rayleigh wave content when correcting H/V amplitudes.*

### Specific comments

1. In 3rd paragraph of Section 2 (Methods of Analysis), I would suggest you present the methodology from Maresca et al (2006) first, and then present the methodology you are proposing. It would emphasize on the benefits of your method.

I agree with the suggestion of the reviewer - the methodology of Maresca et al (2006) is referenced first now and the paragraph reads accordingly:

*Maresca et al (2006) use a different approach and compare the distribution of propagation and polarisation directions in four different frequency bands for two arrays in the Colfiorito Basin, Italy. For one array, they find no clear patterns, while for the other, the approximately normal angle between the propagation and polarisation directions indicates the presence of Love waves in the noise wavefield. This study is based on the same idea. Our observations indicate that the noise wavefield around the H/V peak often exhibits energy concentrations related to distinct sources. These are used to estimate the relative content of Love and Rayleigh waves from the propagation directions obtained by frequency-wavenumber (FK) analysis and the horizontal polarisation directions. In contrast to the study by Maresca et al (2006), I introduce a quantitative estimate of the relative amount of Love and Rayleigh waves in the wavefield and study the variability of this quantity with frequency, with a special emphasis on the H/V peak frequency. Details of the proposed method are given below.*

2. In the 1st paragraph of Section 2.4 (page 4), why is the criterion of the maximum value of the histogram fixed at 2.2 times the averaged value? Why do you use 15deg as tolerance expected for Rayleigh or Love waves? How did you establish these limits?

The criteria, and especially the selection of the exact values used, are explained in more detail now. These values are derived from the actual data, both synthetic and measured, especially from the distributions of angular shift between propagation and polarisation directions as depicted in Fig. 1. The choice of the amplitude threshold level is motivated by the necessity of excluding distributions that show randomly placed, isolated amplitude peaks (e.g. Fig. 1 a)) as well as those that look more uniform (e.g. Fig. 1 d)). The width of regions which are supposed to contain the maximum of the distribution is based on the half-width of exemplary distributions (e.g. Fig. 1 b) ). This choice is not as critical as the threshold level, however, as most distributions that fail to meet the criteria fail already at the first one. Tests with different choices of the exact values used have show that, for both, synthetic and measured data, the results for  $\alpha$  are themselves robust against variations, while the estimates of the standard deviations and the frequency bands for which measurements are possible may change. However, a restrictive choice of the threshold parameters is necessary to exclude spurious estimates based on arbitrary distributions as they are impossible to identify later on.

3. Section 2.4, last sentence of 1st paragraph, you state that "the vast majority of rejected points are due to the filtering by the first criterion". Could you further comment on the implication of this result on the use of the methodology proposed? It seems to be an important restriction to the methodology, would be important to further understand the limits of application of the method.

I included additional explanation to the text, stating that this observation implies that most data that are rejected are deselected because no clear maximum in the angular distribution between polarisation and propagation angles is found. This limits the application of the method in cases of a wavefield that is composed of several simultaneously acting sources or truly random. The text reads now,

*In applications to real data, the vast majority of the points rejected are the result of filtering using the first criterion, an indistinct maximum in the distribution of the angular shifts. This implies that for actual field cases, at least over the measurement intervals used in this study, there are always frequency bands that do not contain single dominant source regions, but rather random wavefields, which limits the applicability of this method. Rejected points are mainly at the high and low ends of the considered frequency band and thus also exhibit a correlation with the limited resolution of the arrays. Rejections are rarely necessary for the synthetic datasets, if at all.*

4. Page 5, Section 3.1.1, it is hard to understand where to look on Table 2. Maybe just reformulate to better direct the reader to the appropriate part of the Table to consider.

References to Tab. 2 in Section 3.1.1 are reformulated to clarify that the reader should consider the uppermost part of the Table.

*Fig. 3 shows the results of the H/V calculations for the two synthetic data sets. As listed in the upper part of Tab. 2 under the label "Synthetics", the maximum amplitude,  $A_0$ , of the H/V peak depends on the contribution of Love waves to the wavefield. It is significantly higher (12.2 vs. 6.2) in the case of randomly oriented source vectors (represented by "L & R FM" in Tab. 2) compared to purely vertical vector sources (described as "R FM" in Tab. 2), which illustrates the Love wave contribution to the H/V peak.*

In addition, I changed the caption of Table 2 to include that the topmost two rows refer to the synthetic datasets.

5. Figure 3, can't you plot the averaged expected HV curves after corrections for the frequency-dependent Love wave contribution? You plot the statistical range of the corrected H/V, but the averaged H/V curve is an important information to plot, as it is the statistical expectation.

I agree that including the correction for the average frequency-dependent value of the Love wave contribution helps to illustrate the benefits of the proposed method. Figure 3 now contains the H/V curve after correcting for the average values of the frequency-dependent Love wave contribution, estimated from both FKPA. Additional discussion is included in the text as well.

6. Page 6, 1st paragraph of 2nd column, starting by "As an independent test of these results.", you describe the corrections determined by FKPA to correct H/V for the contribution of Love waves. how do you proceed with the corrections? It is not clear to me how the corrections to the HV curve are achieved. maybe just a sentence summarizing that step would help. You also mention spectral smoothing as a possible cause explaining the discrepancy between the original and corrected H/V curves. Could there be any physical explanation to this discrepancy? Please comment.

A short explanation on how the H/V curves are corrected for the frequency-dependent values of Love wave content of the wavefield determined by FKPA or MSPAC is added to section 2.4 on the methodology:

*The obtained values of  $\alpha$  can be used to correct the measured H/V curves for the influence of Love waves. Following Fäh et al (2003), the amplitude of the horizontal component of the surface wave wavefield is described by vector addition of the Rayleigh wave contribution,  $R$ , on the radial component and the Love wave contribution,  $L$ , on the transverse component. If  $R$  is normalised to 1, the reduction factor,  $c$ , is obtained by*

$$c = \sqrt{L^2 + R^2}$$

*The dependency on  $\alpha$  can then be expressed by*

$$c = \sqrt{\left(\frac{100 - \alpha}{\alpha}\right)^2 + 1^2}$$

*For the case of equal Love and Rayleigh contributions to the wavefield, the above equations lead to a value of  $\sqrt{2}$  for  $c$ . Division of the measured H/V curves by  $c$  results in a correction for the Love wave contribution to the horizontal components.*

The reference to spectral smoothing as a cause for the observed discrepancy is removed from the text. As shown in the new version of Fig. 3, the theoretical ellipticity of the fundamental mode Rayleigh wave (dashed black line) agrees nearly perfectly with the H/V curve calculated for a synthetic pure Rayleigh wave wavefield. This can be taken as an argument against spectral smoothing influencing the H/V curve in any significant way. The discrepancy that is still observed might, as stated in the text, be inherent to the way the synthetic wavefield is generated.

7. Page 6-7, Section 3.1.2. Hard to understand what sources are left in the model. you mention you have background sources distributed at distances of 0m to 2.2km from the array centre, and you then mention about the importance of removing close sources. It is confusing, maybe some rewording would help. Maybe adding a sentence to remind the reader the range of distances the sources were generated in the 1st place (90m to 2.2km) to better understand the difference in both experiments.

I reformulated the beginning of section 3.1.2 to clearly state the difference between the modelling reported in this section and the original model described in Section 3.1.1.:

*To investigate the influence of the source-free region in close vicinity to the recording stations, a dataset with background sources randomly distributed between 0 m and 2.2 km from the array centre was created. In contrast to the case presented before (3.1.1), where no sources are located closer than 90 m to the array centre, this synthetic example includes background sources located within the array. Adding close sources significantly increases the curvedness of the recorded wavefronts. This violates the assumption made in FK processing, of a plane wave front moving across the array.*

8. Page 7, Section 3.1.3 (Higher Modes) doesn't bring much additional information. Would consider removing, or rewriting to better state the importance of the results from higher modes.

I added some additional sentences to Section 3.1.3 to describe the potential importance of higher modes in the actual (measured) ambient vibration wavefield on the one hand and the difficulties that these might pose for estimating the Love wave content with the MSPAC method on the other hand. This in return implies that the FKPA method has potential benefits over MSPAC when applied to a multi-modal wavefield as the modelling presented in Section 3.1.3 shows that it is not compromised by the presence of higher modes. Because of these two points, I do consider Section 3.1.3 important and did not remove it. The new text reads:

*The actual distribution of various modes in the ambient vibration wavefield is rarely studied and depends on local site and source properties (Bonney-Claudet et al, 2006). Several studies do, however, indicate that higher modes may be of importance, for example*

*in obscuring the trough in the H/V curve associated with the Rayleigh fundamental mode Airy phase, or for the inversion of dispersion curve data (Bonney-Claudet et al, 2006). The conventional implementation of SPAC (Aki, 1957) and MSPAC techniques are confined to the resolution of single mode Rayleigh and Love waves (Bonney-Claudet et al, 2008). Accordingly, a theoretical investigation using the MSPAC method (Köhler et al, 2007) indicates that estimates of  $\alpha$  deteriorate at frequencies where higher modes dominate the wavefield. On the other hand, because FK methods have the potential to resolve several surface wave modes simultaneously (Poggi and Fäh, 2009), the FKPA method might have advantages over the MSPAC method at these conditions. A dataset that contains both fundamental and higher modes was created to investigate this point.*

9. Page 7, Section 3.1.4, add that 2nd source region on Figure 2, to help the reader quickly localize that region. The low resolution of the method when there is good azimuthal coverage of sources is an important restriction. An additional figure showing the smearing between the two main directions of propagation and polarization would be important to show that limit.

As suggested by the reviewer, I added the 2nd source region to Figure 2. Besides, Fig. 8 was added to show the smearing between the four different polarization directions for two sources for both Love and Rayleigh waves in the ambient vibration wavefield, and is discussed in Section 3.1.4.

10. Page 9, 1st paragraph. Why do you make reference to Table 4 before Table 3? It is confusing for the reader. It would be preferable to invert these two tables.

The two tables are swapped in order to comply with the references in the text.

11. Figure 16 is very complex to understand. There is too much information to digest, with the symbols and color code changing from one panel to the other. I would suggest finding an alternative way to present the results.

To reduce the information contained in former Fig. 16 (now Fig. 20), the results for sites Nestos and Athens, which are discussed in detail, are shown now in Fig. 14 and 18 together with the corrected H/V curves. These two Figures show the good correlation between results obtained with different array sizes at the same site. The results concerning temporal variability in the H/V curves as measured at the site Colfiorito are also presented in an additional section, 3.2.3., and in Fig. 19 now, to make them easier accessible. Besides, for two sites (Cerreto di Spoleto and Norcia), results were only available at a few isolated frequencies. A display of these results vs. the whole analysed frequency band is not warranted, so they were also excluded from former Fig. 16 (current Fig. 20). This leaves less individual panels. In addition, colour is completely removed from this figure, which is simply showing the comparison between results from FKPA and MSPAC with frequency for all other sites now. I hope this sufficiently simplifies this Figure and improves the reception.

12. Some results are presented in the Conclusion section. I would suggest moving the paragraphs starting by "For the site of Colfiorito, ..." (page 10-11), "At other sites, only shorter time ranges..." (page 11), and "The data from the NERIES..." (page 11) to the results section. These three paragraphs present results and do not belong to the conclusion section.

The results regarding temporal variability in the longer-term measurements at Colfiorito are now moved to a new part of the Results section, 3.2.3. Similarly, the other paragraphs mentioned by the reviewer are removed from the Conclusion section and moved into the Results section.

## Reviewer #2

The following short revision should be carried out: At the beginning of the introduction with "...this peak occurs is empirically found to correlate with the fundamental resonance frequency..." a sentence like "It was found theoretically by Malischewsky and Scherbaum (2004) that this coincidence is all the better, the higher the impedance contrast between layer and half-space is." should be inserted for completeness.

I inserted a sentence referring to the work by Malischewsky and Scherbaum (2004) into the introduction:

*For the case of a single low-velocity layer over a halfspace, Malischewsky and Scherbaum (2004) show theoretically that this correlation is better, the higher the impedance contrast between the layer and the half-space.*

## References

Aki K (1957) Space and time spectra of stationary stochastic waves, with special reference to microtremors. *Bull Earthq Res Inst* 35:415–457

Bonnefoy-Claudet S, Cotton F, Bard PY (2006) The nature of noise wavefield and its application for site effects studies A literature review. *Earth-Science Reviews* 79:205–227, doi:10.1016/j.earscirev.2006.07.004

Bonnefoy-Claudet S, Köhler A, Cornou C, Wathelet M, Bard PY (2008) Effects of Love waves on microtremor H/V ratio. *Bull Seism Soc Am* 98(1):288–300, doi:10.1785/0120070063

Fäh D, Kind F, Giardini D (2003) Inversion of local S-wave velocity structures from average H/V ratios, and their use for the estimation of site-effects. *J Seism* 7:449–467

Köhler A, Ohrnberger M, Scherbaum F, Wathelet M, Cornou C (2007) Assessing the reliability of the modified three-component spatial autocorrelation technique. *Geophys J Int* 168:779–796, doi:10.1111/j.1365-246X.2006.03253.x

Malischewsky PG, Scherbaum F (2004) Love's formula and H/V-ratio (ellipticity) of Rayleigh waves. *Wave Motion* 40:57–67, doi:10.1016/j.wavemoti.2003.12.015

Maresca R, Galluzzo D, Del Pezzo E (2006) H/V spectral ratios and array techniques applied to ambient noise recorded in the Colfiorito Basin, Central Italy. *Bull Seism Soc Am* 96(2):490–505, doi:10.1785/0120050057

Poggi V, Fäh D (2009) Estimating Rayleigh wave particle motion from three-component array analysis of ambient vibrations. *Geophys J Int* Doi:10.1111/j.1365-246X.2009.04402.x



[www.journalexperts.com](http://www.journalexperts.com)

## American Journal Experts Editorial Certification

This document certifies that the manuscript titled "Love wave contribution to the ambient vibration H/V amplitude peak observed by array measurements" was edited for proper English language, grammar, punctuation, spelling, and overall style by one or more of the highly qualified native English speaking editors at American Journal Experts. Neither the research content nor the authors' intentions were altered in any way during the editing process.

Documents receiving this certification should be English-ready for publication - however, the author has the ability to accept or reject our suggestions and changes. To verify the final AJE edited version, please visit our verification page. If you have any questions or concerns over this edited document, please contact American Journal Experts at [support@journalexperts.com](mailto:support@journalexperts.com)

**Manuscript title:** Love wave contribution to the ambient vibration H/V amplitude peak observed by array measurements

**Authors:** Brigitte Endrun

**Key:** A354-E212-E9FD-B869-1C22

This certificate may be verified at [www.journalexperts.com/certificate](http://www.journalexperts.com/certificate)

American Journal Experts is an association of Ph.Ds and Ph.D. graduate students from America's top 10 research universities. Our editors come from nearly every research field and possess the highest qualifications to edit research manuscripts written by non-native English speakers. We provide the quickest turnaround times at the lowest prices in the industry. For more information, please visit [www.journalexperts.com](http://www.journalexperts.com), or for volume discounts for academic journals, please contact us by email at [sales@journalexperts.com](mailto:sales@journalexperts.com)